Astronomy & Astrophysics manuscript no. CALIFA_DR2
September 17, 2014

CALIFA, the Calar Alto Legacy Integral Field Area survey

III. Second public data release⋆

R. García-Benito[1], S. Zibetti[2], S. F. Sánchez[3], and et al.

(Affiliations can be found after the references)

ABSTRACT

This paper describes the Second Public Data Release (DR2) of the Calar Alto Legacy Integral Field Area (CALIFA) survey. It includes 200 objects, including the previous 100 of the First Public Data Release (DR1), from the eventually 600 nearby ($0.005 < z < 0.03$) galaxies of the final sample, obtained with the integral-field spectrograph PMAS/PPak mounted on the 3.5 m telescope at the Calar Alto observatory. Two different spectral setups are available for each galaxy, (i) a low-resolution V500 setup covering the nominal wavelength range 3745–7500 Å with a spectral resolution of 6.0 Å (FWHM), and (ii) a medium-resolution V1200 setup covering the nominal wavelength range 3650–4840 Å with a spectral resolution of 2.3 Å (FWHM). Both setups together contain over 2 million spectra, with a wide range coverage of properties in the Color-Magnitude diagram, stellar mass, ionization conditions and homogeneous distribution of morphological types. The data release includes improved spectrophotometric calibration, registering and spatial resolution. The spectrophotometric calibration is better that 6% and the median spatial resolution is 2.″6. The second data release is available at `http://califa.caha.es/DR2`.

Key words. techniques: spectroscopic - galaxies: general - surveys

1. Introduction

The Calar Alto Legacy Integral Field Area (CALIFA) survey (Sánchez et al. 2012a, hereafter S12) is an ongoing large project of the Centro Astronómico Hispano-Alemán at the Calar Alto observatory to obtain spatially resolved spectra for 600 local ($0.005< z <0.03$) galaxies by means of integral field spectroscopy (IFS). CALIFA observations started in June 2010 with the Potsdam Multi Aperture Spectrograph (PMAS, Roth et al. 2005), mounted to the 3.5 m telescope, utilizing the large (74″×64″) hexagonal field-of-view (FoV) offered by the PPak fiber bundle (Verheijen et al. 2004; Kelz et al. 2006). Each galaxy is observed using two different setups, an intermediate spectral resolution one (V1200, $R \sim 1650$), that cover the blue range of the optical wavelength range (3700-4700Å), and a low-resolution one (V500,$R \sim 850$, that covers the first octave of the optical wavelength range (3750-7500Å). A diameter-selected sample of 939 galaxies were drawn from the 7th data release of the Sloan Digital Sky Survey (SDSS DR7, Abazajian et al. 2009) which is described in (W14, Walcher et al. 2014). From this mother sample the 600 target galaxies are randomly selected.

Combining the techniques of imaging and spectroscopy through optical IFS provides a more comprehensive view of individual galaxy properties than any traditional survey. CALIFA-like observations were collected during the feasibility studies (Mármol-Queraltó et al. 2011; Viironen et al. 2012) and the PPak IFS Nearby Galaxy Survey (PINGS, Rosales-Ortega et al. 2010), a predecessor of this survey. First results based on those datasets already explored their information content (Sánchez et al. 2011; Rosales-Ortega et al. 2011; Alonso-Herrero et al. 2012; Sánchez et al. 2012b; Rosales-Ortega et al. 2012, e.g.). CALIFA can therefore be expected to make a substantial contribution to our understanding of galaxy evolution in various aspects including, (i) the relative importance and consequences of merging and secular processes; (ii) the evolution of galaxies across the color-magnitude diagram; (iii) the effects of the environment on galaxies; (iv) the AGN-host galaxy connection; (v) the internal dynamical processes in galaxies; and (vi) the global and spatially resolved star formation history of various galaxy types.

Compared with previous IFS surveys, e.g., Altas3D (Cappellari et al. 2011) or DMS (Bershady et al. 2010), and on-going ones, like MaNGA (Law & MaNGA Team 2014) and SAMI (Croom et al. 2012), CALIFA offers an unique combination of (i) a sample covering a wide range of morphological types in a wide range of masses, sampling the Color-Magnitude diagram for $M_g > -18$ mag; (ii) a large FoV, that guarantees to cover the entire optical extension of the galaxies up to $2.5r_e$ for an 80% of the sample; and (iii) an accurate spatial sampling, with a typical spatial resolution of ∼1 kpc for the entire sample, which allows to optical spatial resolved spectroscopic properties of most relevant structures in galaxies (spiral arms, bars, bulges, H II regions...). The penalty for a better spatial sampling of the galaxies is the somehow limited number of galaxies in the survey, compared with other on-going IFU surveys (e.g., MaNGA and SAMI). In terms of the spectral resolution, only the blue wavelength range is sampled with a similar spectral resolution than these two other surveys.

Different science goals have been already addressed using the data from the CALIFA survey: (i) New techniques has been developed to understand the spatially resolved star formation histories (SFH) of galaxies (Cid Fernandes et al. 2013, 2014). We found the solid evidence that mass-assembly in the typical galaxies happens from inside-out (Pérez et al. 2013). The SFH of

⋆ Based on observations collected at the Centro Astronómico Hispano Alemán (CAHA) at Calar Alto, operated jointly by the Max-Planck-Institut für Astronomie (MPIA) and the Instituto de Astrofísica de Andalucía (CSIC)

bulges and early-type galaxies are fundamentally related to the total stellar mass, while for disk galaxies it is more related to the local stellar mass density (González Delgado et al. 2014b,a); (ii) We developed new tools to detect and extract the spectroscopic information of H II regions (Sánchez et al. 2012b), building the largest catalog currently available (~6,000 H II regions and aggregations). This catalog has been used to define a new oxygen abundance calibrator anchored with electron temperature measurements (Marino et al. 2013). From these, we explored the proposed dependence of the Mass-Metallicity relation with SFR (Sánchez et al. 2013), and the local Mass-Metallicity relation (Rosales-Ortega et al. 2012). We found that all galaxies in our sample present a common abundance radial gradient with a similar slope when normalized to the effective radius (Sánchez et al. 2014), which agrees with the proposed inside-out scenario for galaxy growth. This characteristic slope is independent of the properties of the galaxies, and in particular of the presence or absence of a bar, contrary to previous results. More recently, this result has been confirmed by the analysis of the stellar abundance gradient in the same sample (Sanchez-Blazquez et al. 2014); (iii) We explore the origin of the low intensity, LINER-like, ionized gas in galaxies. These regions regions are clearly not related to star-formation activity, or to AGN activity. They are most probably related to post-AGB ionization in many cases (Kehrig et al. 2012; Singh et al. 2013; Papaderos et al. 2013) (iv) We explore the aperture and resolution effects on the data. CALIFA provides a unique tool to understand the aperture and resolution effects in larger single-fiber (like SDSS) and IFS surveys (like MaNGA, SAMI). We explored the effects of the dilution of the signal in different gas and stellar population properties (Mast et al. 2014), and proposed an new empirical aperture correction for the SDSS data (Iglesias-Páramo et al. 2013); (v) The different described dataproducts were also used to study the progenitors of Super Novae of different types, by analysing the local properties of the ionized gas and underlying stellar population at the location where former supernovae have exploded (Galbany et al. 2014); (vi) CALIFA is the first IFU survey that allows gas and stellar kinematic studies for all morphologies with enough spectroscopic resolution to study (a) the kinematics of the ionized gas (Garcia-Lorenzo et al. 2014), (b) the effects of bars in the kinematics of galaxies (Barrera-Ballesteros et al. 2014); (c) the effects of the interaction stage on the kinematic signatures (Barrera-Ballesteros et al., submitted), (d) measure the Bar Pattern Speeds in late-type galaxies (Aguerri et al., submitted), (e) extend the measurements of the angular momentum of galaxies to previously unexplored ranges of morphology and ellipticity (Falcón-Barroso et al., in prep.).

In this article, we introduce the second data release (DR2) of CALIFA which grants public access to high-quality data for a set of 200 galaxies (400 datacubes). This DR increases by a factor two the amount of data delivered in DR1 (H13, Husemann et al. 2013). DR1 opened CALIFA to the community, and allowed to explore different science cases do not addressed by the collaboration (e.g. Holwerda & Keel 2013; De Geyter et al. 2014; Martínez-García et al. 2014; Davies et al. 2014). The properties of the galaxies in the DR2 sample are summarized in Sect. 2. We describe the data characteristics (Sect. XX), data structure (Sect. XX), and data quality (Sect. 5) of the distributed CALIFA data as essential information for any scientific analysis. Several interfaces are available to access the CALIFA DR2 data, which are introduced in Sect. 6.

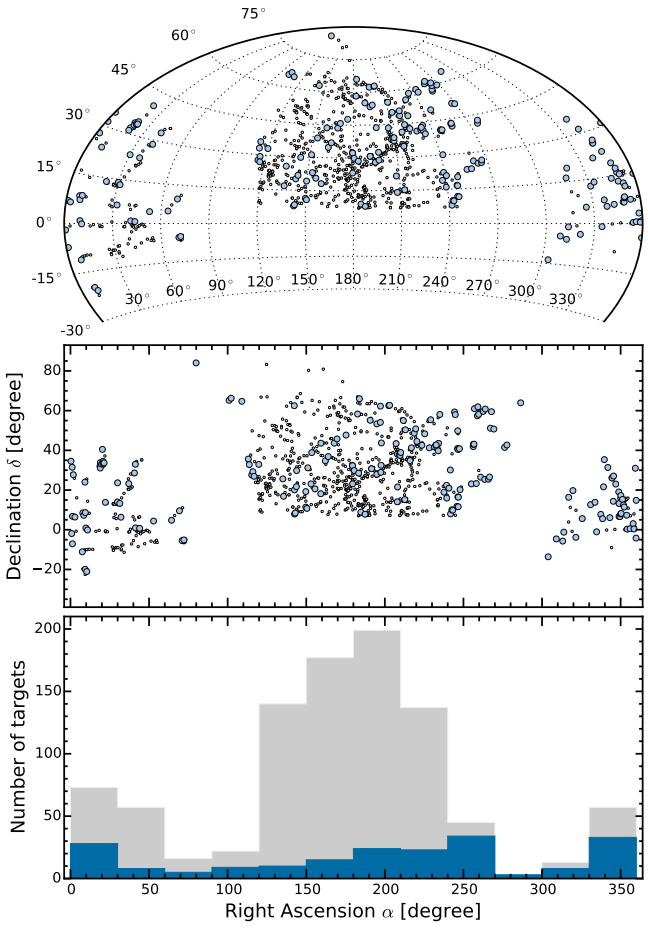

Fig. 1. Distribution on the sky of galaxies in the CALIFA mother sample (black dots) and CALIFA DR2 sample (blue filled symbols). The upper panel shows the distribution in an Aitoff projection in J2000 Equatorial Coordinates (cut off at $\delta = 30°$, below which the sample did not extend), while the middle panel is plotted in cartesian system. The lower panel shows both samples as a function of right ascension. The number distribution in bins of 30° along the right ascension is shown in the lower panel for the mother sample (gray area) and the DR2 sample (blue shaded area).

2. The CALIFA DR2 sample

The CALIFA "mother sample" (MS) consists of 939 galaxies, drawn from SDSS DR7. The main criteria for the target selection are: angular isophotal diameter ($45'' < isoA_r < 79.2''$) of the galaxies[1]; redshift range $0.005 < z < 0.03$; cut in Galactic latitude to exclude the Galactic plane ($b > 20°$ or $b < 20°$) and flux limit of $petroMag_r < 20$; declination limit to $\delta > 7$ deg. Redshift limits were impose so that the sample would not be dominated by dwarf galaxies and also ensure to observe all interesting spectral features with a fixed spectral setup of the instrument. Redshift information was taken from SIMBAD for all galaxies where SDSS DR7 spectra were unavailable. The cut in declination was chosen to reduce problems due to differential atmospheric refraction (DAR) and PMAS flexure issues, but was not applied to the SDSS Southern area due to the sparsity of objects in this region. The reader is referred to W14 for a com-

[1] $isoA_r$ is the isophote major axis at 25 magnitudes per square arcsecond in the r band. For other SDSSpipeline parameters meaning, the reader is referred to the DR7 webpage: http://skyserver.sdss.org/dr7/en/help/browser/browser.asp

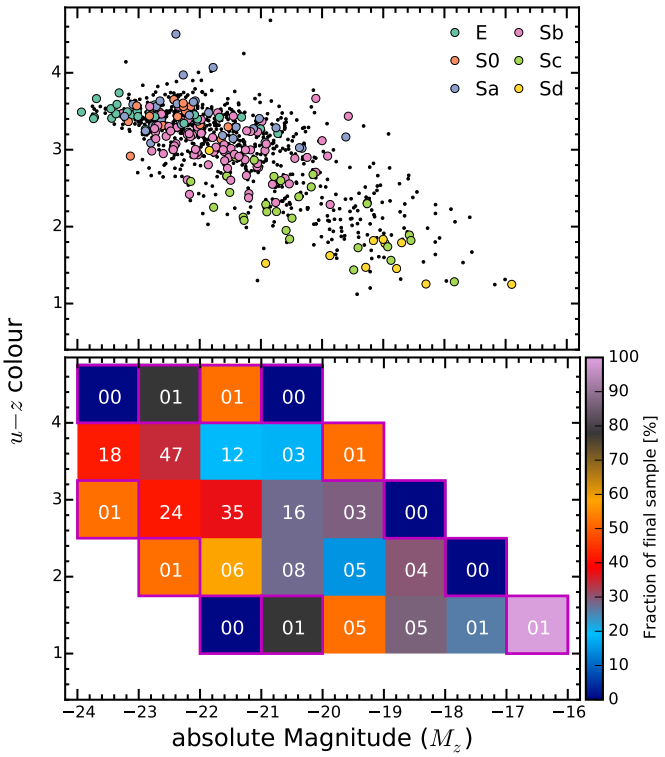

Fig. 2. *Upper panel:* Distribution of CALIFA galaxies in the $u-z$ vs. M_z color-magnitude diagram. Black dots denote galaxies in the CALIFA MS (S12, W14) and colored symbols indicate CALIFA DR2 galaxies. Different colors account for the morphological classification of galaxies which range from ellipticals (E) to late-type spirals (Sd). *Lower panel:* Fraction of galaxies in the DR2 sample with respect to the expected final CALIFA sample distribution (600 objects) in bins of 1 mag in M_z and 0.75 mag in $u-z$. The total number of galaxies per bin in the DR2 sample is shown in each bin. Bins for which the number of galaxies in the MS is less than 5 are prone to low-number statistics and enclosed by a magenta square for better identification.

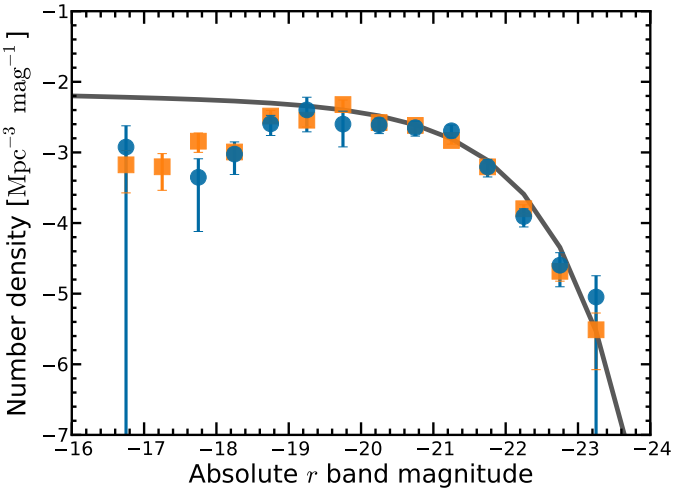

Fig. 3. Luminosity functions in the r band of the CALIFA MS (blue points) and the DR2 sample (orange squares). Error bars represent Poissonian uncertainties. The (grey) line shows the Schechter fit to the LF of Blanton et al. (2005).

prehensive characterization of the CALIFA mother sample and a detailed evaluation of the selection effects implied by the chosen selection criteria. From the CALIFA MS, 600 galaxies are randomly selected for observation purely based on visibility, and we refer to these galaxies as the virtual final CALIFA sample hereafter.

The 200 DR2 galaxies, which includes the first 100 galaxies of DR1, were observed in both spectral setups from the start of observations in June 2010 until December 2013. We list these galaxies in Table 1 together with their primary characteristics. The distribution of galaxies in the sky follows the underlying SDSS footprint (Fig. 1). The number of galaxies in DR2 is not homogeneous as a function of right ascension, α(J2000), and has three mean clear peaks around $\alpha \sim 15°$, 255°and 345°. All three peaks are located in the same season run, in the period from April to October. As noted in H13, there was a downtime of the 3.5 m telescope from August 2010 until April 2011 due to operational reasons at the observatory, which delayed the survey roughly by 8 months. In addition to this, due to scheduling matters, a large part of the granted time was allocated in summer seasons. Regardless of the observing time issue, the distribution of physical properties for DR2 is nearly random, as expected, and covers galaxies with a wide range of properties as discussed below.

Figure 2 shows the distribution of galaxies in the color-magnitude diagram. It is clearly seen that the DR2 sample covers nearly the full range of the CALIFA MS. On average, the DR2 targets comprises ~37% per color-magnitude bin of the total 600 objects when CALIFA is completed. The deficit of low luminosity galaxies with intermediate colors noted in DR1 has improved slightly. Fluctuations can be explained by the effect of low number statistics, especially within those where the mother sample contains few galaxies. This point is highlighted in Figure 2 and makes clear the need to further increase the numbers to the full CALIFA sample to obtain enough galaxies in each bin for a meaningful multi-dimensional statistical analysis.

One important test to be made is whether the number density of galaxies estimated from the CALIFA sample is in accordance with other surveys. Fig. 3 shows the r band luminosity function (LF) of the DR2 sample as compared to the mother sample and the reference SDSS sample of Blanton et al. (2005). The reader is referred to W14 for all technical details on how the LFs is obtained and for the explanation of the turnover of the LF at $M_r \approx -18.6$. It should be noted that DR2 sample already reproduces very closely the LF in most of its magnitude bins.

One important characteristics of the CALIFA MS is that it contains galaxies of all morphological types. Galaxy morphologies were inferred by combining the independent visual classifications of several collaboration members as described in W14. Fig. 4 shows the bar strength histogram as well as the fraction of DR2 galaxies with respect to the expected final sample distribution for different morphological types grouped into elliptical, lenticular and spiral galaxies (and subtypes). A more detailed classification of ellipticals (from 0 to 7) is available, but we do not distinguish between them here because of the low number of galaxies per elliptical subtype within DR2. From 200 galaxies in DR2, 18 have been classified as ongoing mergers (of any type). As clearly seen in Fig. 4, the fraction of DR2 galaxies with respect to the expected final sample is almost constant for all types, implying that the DR2 coverage seems to be consistent with a random selection. Axis ratios (b/a) were measured from the SDSS r band image from growth curve analysis by calculating light moments after proper sky subtraction and masking of foreground stars (see W14 for details). The fractions of axis ratios, which can be used as a proxy of the inclination of spiral galaxies, covered by the DR2 sample is homogeneous with

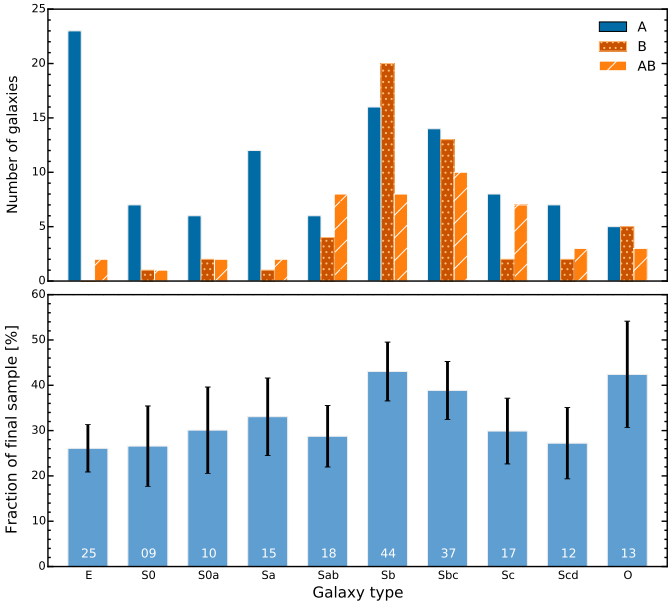

Fig. 4. The distribution of visually classified morphological types in the DR2 sample. We divide the galaxies into ellipticals (E), several common spiral classification (from S0 to Scd) and the *other* group "O" which includes Sd, Sdm, Sm and I (only one) types. *Upper panel:* Bar strength histogram, where A stands for non-barred, B for barred and AB if unsure. *Lower panel:* The fraction of galaxies in the DR2 sample with respect to the expected final CALIFA sample distribution. The total number of galaxies in the DR2 for each morphology type is written on each bar. Error bars are computed from the Poisson errors of the associated DR2 number counts. The morphological distribution of the DR2 sample lies close to that of the mother sample.

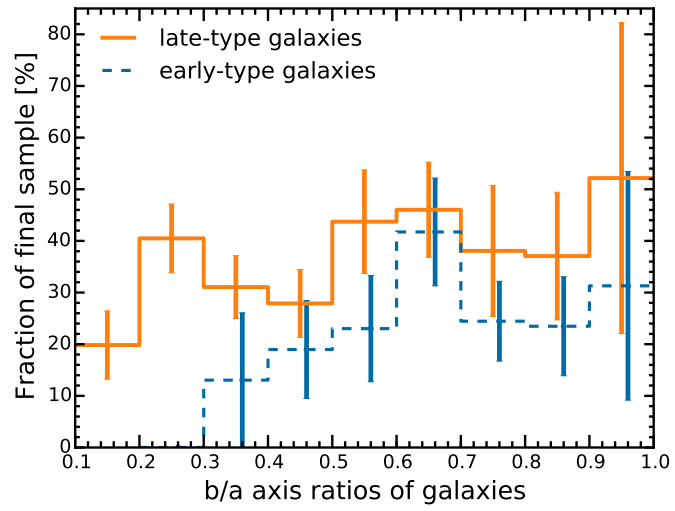

Fig. 5. The fraction of galaxies in the DR2 sample with respect to the expected final CALIFA sample distribution, as a function of the isophotal axis ratio (b/a). Galaxies were separated into early-type galaxies (E+S0) and late-type galaxies (Sa and later). The CALIFA MS does not include any elliptical galaxies with $b/a < 0.3$ or any spiral galaxies with $b/a > 0.9$. Error bars are computed from the Poisson errors of the associated DR2 number counts.

respect to the final sample (Fig. 5). We also quantified that the morphology and the axis-ratio distribution of DR2 is consistent with being randomly drawn from the CALIFA mother sample by means of a Kolmogorov-Smirnov test with > 95% confidence.

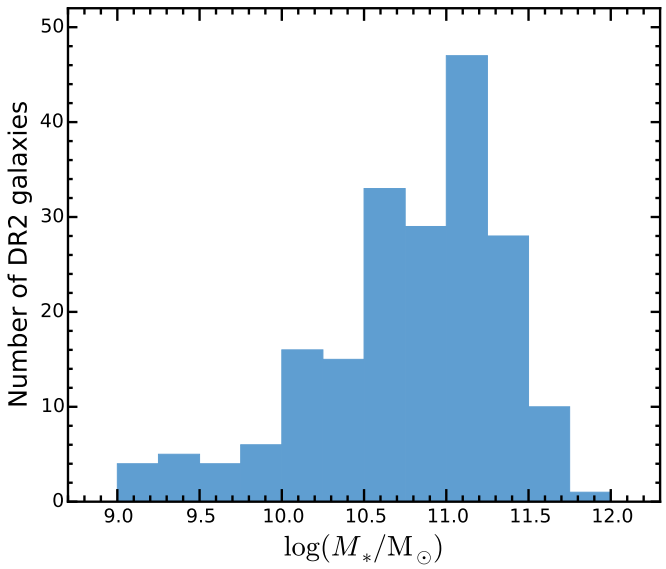

Fig. 6. Distribution of stellar masses in the DR2 sample. The stellar masses have been determined from the CALIFA data using spectral fitting techniques (see text for details).

In Fig. 6, we present the distribution of stellar masses for the DR2 galaxies. Galaxy stellar masses are from González Delgado et al. (2014a), and they have been estimated following the process described in Pérez et al. (2013), Cid Fernandes et al. (2013, 2014) and González Delgado et al. (2014b). These masses account for M/L ratio spatial variations and stellar extinction. In short, we use the STARLIGHT code (Cid Fernandes et al. 2005) to fit each spectrum extracted from the data cube with a combination of SSP spectra from the Granada (González Delgado et al. 2005) and MILES (Vazdekis et al. 2010) models, that cover the full metallicity range of the MILES models (log Z/Z$_*$ from -2.3 to +0.33), and ages from 0.001 to 14 Gyr. We assume a Salpeter IMF. The DR2 galaxies cover intermediate to high-mass galaxies, including at least 10 galaxies per 0.25 dex bin between 10^{10} and $10^{12} M_\odot$ and a median value close to 10^{11}M$_\odot$. The asymmetric distribution is expected from the distribution in absolute magnitudes (see Fig. 2) and is inherited from the CALIFA mother sample due to its selection criteria (see W14 for details).

Another general "*panoramic view*" of the characteristics of the DR2 sample is the one shown in Fig. 7. Some of the main properties plotted in 2D maps for 169 galaxies[2] of the DR2 sample are placed in small hexagons shaping all together a CALIFA-like FoV. The galaxies have been ordered by absolute magnitude in r band (a proxy for the stellar mass) from top to bottom and right to left (top right galaxy being the one with lowest absolute magnitude and bottom left one the highest). Some of the properties have been derived using different pipelines analysis within the collaboration. Stellar properties like ages and mas surface density were derived from the STARLIGHT code (see references in the paragraph dealing with the distribution of stellar masses above) and emission lines and gas properties from FIT3D (Sánchez et al. 2007). This plot is only intended to demonstrate the diversity of the DR2 sample.

3. Data processing and error propagation

For the sake of completeness, we provide here a brief summary of the instrument layout and observing strategy. All the details

[2] Maximum filled regular hexagon.

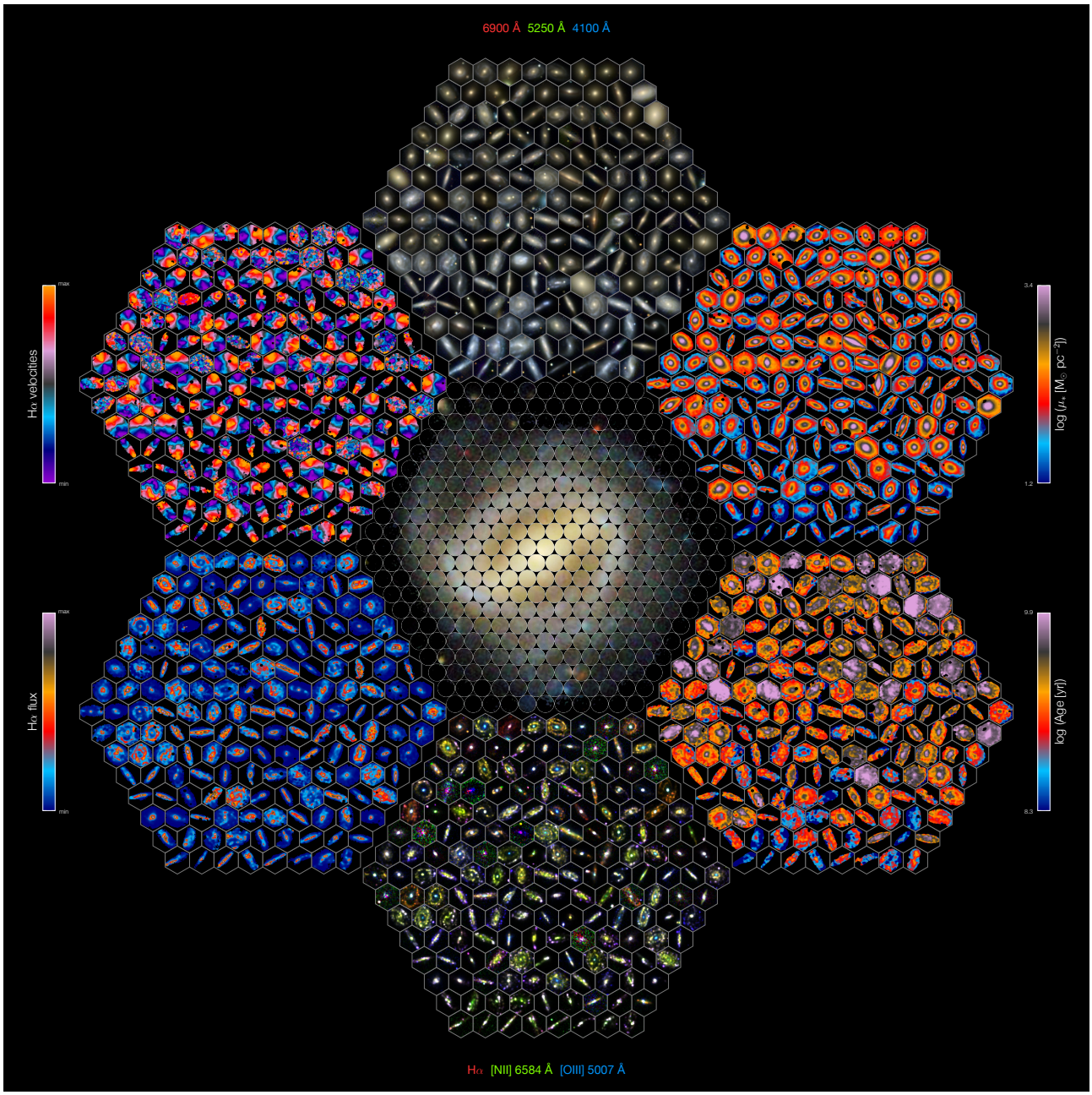

Fig. 7. CALIFA "*panoramic view*" (also CALIFA's "*Mandala*") representation. Main physical properties (all of them derived from the CALIFA data cubes) of a subsample of 169 galaxies extracted randomly from DR2. Shown here are 1) broad band images (center up; central wavelength 6900 Å, 5250 Å, and 4100 Å), 2) stellar mass surface densities (upper right), 3) ages (lower right), 4) narrow band images (lower center; emission lines: Hα, [N II] 6584 Å, and [O III] 5007 Å), 5) Hα emission (lower left) and 6) Hα kinematics (upper left). The CALIFA logo is placed at the central hexagon.

can be found in S12. The PPak fiber bundle of the PMAS instrument has a field-of-view (FoV) of 74″× 64″. There are in total 382 fibers, distributed in 3 different groups. The PPak IFU holds 331 "science" fibers in a hexagonal grid with a maximum diameter of 74″while each fiber projects to 2.7″in diameter on the sky. The fiber-to-fiber distance is 3.6 which yields a total filling factor of 0.60. An additional 36 fibers devoted to obtain the surrounding sky are distributed in six bundles of 6 fibers each, located following a circular distribution and placed 72″from the center. Finally, there are 15 extra fibers connected to the calibration unit.

Every galaxy in the CALIFA sample is observed in the optical range using two different (overlapping) setups. The V500 low-resolution mode (R ∼ 850) covers the range 3745-7500 Å cbut it is affected by internal vignetting within the spectrograph giving an unvignetted range 4240-7140Å. The blue mid-resolution setup (V1200; R ∼ 1650) covers the range 3400-4840 Å with an unvignetted range 3650-4620 Å. The resolutions quoted are those at the overlapping wavelength range ($\lambda \sim 4500$ Å). In order to reach a filling factor of 100% across the FoV, a 3-pointing dithering scheme is used for each object. The exposure time per pointing is fixed. V1200 observations are carried out during dark nights with a exposure time of 1800 s (split in 2 o 3 individual exposures) pointing. V500 observations are taken during grey nights with 900 s per pointing.

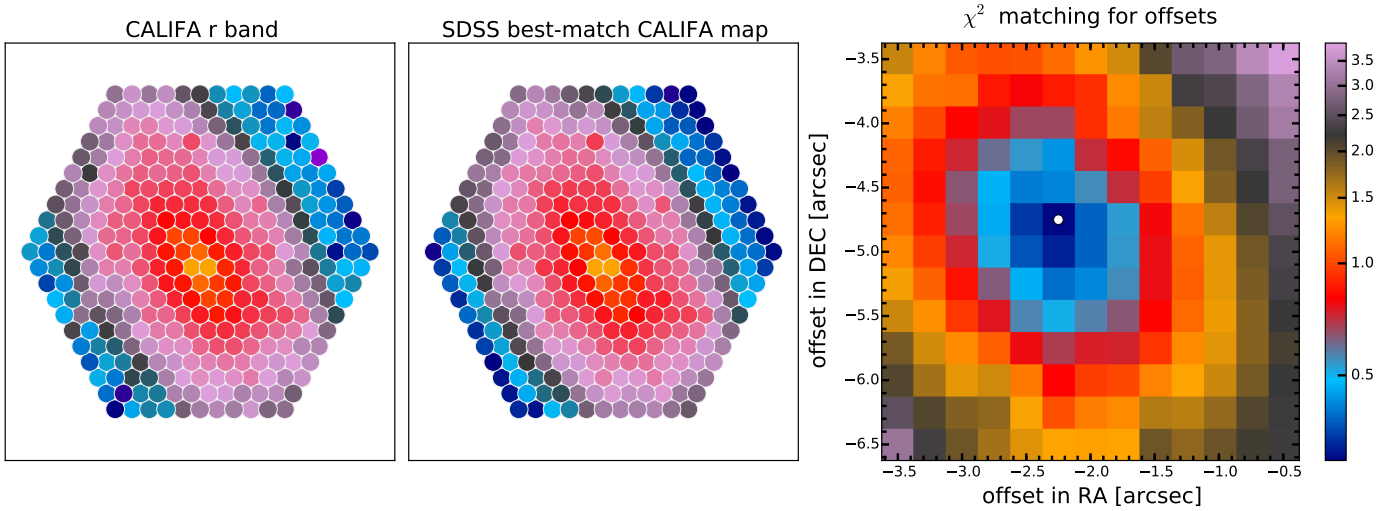

Fig. 8. Example of the registering method for pointing 1 of NGC0496 (ID 45). *Left panel:* Flux map in *r* band for the PPak fibers. *Central panel:* Predicted SDSS flux for each CALIFA fiber estimated using 2.7″ diameter apertures and adopting the PPak layout projected on the SDSS image for the best match according to the χ^2 map. *Right panel:* χ^2 map of the offsets (best offset marked with a white dot).

In the following section we described the new improvements to the CALIFA data reduction pipeline used to produce the DR2 data.

3.1. Improvements on the CALIFA data reduction scheme

As described in H13, since version 1.3c, CALIFA pipeline has a `Python`-based architecture (`Py3D` package). The main drivers for current pipeline version 1.5 are: i) new sensitivity curve for V500 setup obtained from a dedicated calibration program for several CALIFA elliptical galaxies (Husemann et al., in preparation) ii) new registering method comparing individual CALIFA pointings with SDSS images; iii) improve image reconstruction method (cube interpolation). Among others, step ii) also improves the absolute photometric matching of the three pointings.

The new version starts with the RSS files of the three individual pointings after sky subtraction produced by pipeline v1.3c. The V500 RSS files are then spectrophotometrically re-calibrated with the new sensitivity curve (undoing the v1.3c calibration). A new estimate for the sensitivity curve was necessary because of the severe wavelength-dependent aperture losses for standard stars observations caused by the low filling factor and the large fiber diameter of PPak. We therefore re-observed about two dozen elliptical CALIFA galaxies with the PMAS Lens-Array (LArr) and the V300 grism with a continuous 16″ × 16″ FoV covering the bright center of the galaxy. The details of those observations and its application for coarse fiber IFU spectrograph will be presented in a separate publication (Husemann et al., in preparation), but we briefly outline the concept and application to the CALIFA data here. The PMAS LArr data achieve a robust spectrophotometric calibration because standard star observation do not suffer from aperture losses in this mode and the atmospheric extinction curve was directly estimated for different observing nights. Based on those secondary spectrophotometric standards we derived a new sensitivity curve by comparing the count spectra of the targeted elliptical CALIFA galaxies and the corresponding LArr flux spectra within the same aperture. Since the elliptical galaxy have a smooth surface brightness profile extended over several tens of arcsec, we are much less sensitive for wavelength-dependent aperture losses. Several CALIFA fibers are within the LArr FoV that are all co-added to increase the S/N. To get a good match between the LArr and PPak spectra with additional smooth the PPak spectra to 9Å FWHM to match the resolution of the V300 LArr observation. We smooth the sensitivity curve by a high-order polynomial to create a noise free representation of the sensitivity curve. A master sensitivity curve is derived by average the sensitivity curves independently derived from individual galaxies. We anticipate that the largest uncertainty in the relative spectrometer along wavelengths for CALIFA will be driven by the unknown extinction curve at the time of each CALIFA observation since the average extinction curve derived by Sánchez et al. (2007) is used for all observations.

The next new step consist of a new scheme for estimating the registration of the images, using *r* band for the V500 setup and *g* band for the V1200, and field calibration images of the SDSS DR7. First, the DR7 SDSS images are calibrated using the corresponding calibration file (`fpC` file) and the sky background is subtracted. Then, for each RSS spectrum the magnitude in the corresponding SDSS filter is computed. The predicted SDSS flux for each CALIFA fiber is estimated using 2.7″ diameter apertures and adopting the PPak layout projected on the SDSS image. This layout is displaced in steps in RA and DEC across a search box in the SDSS image. Then a χ^2 map is computed to obtain the best offsets for each pointing taking into account errors in the flux measurements and allowing for a photometric scaling factor between SDSS and the CALIFA observations as an additional parameter. Only fibers with S/N > 3.0 are taking into account in the χ^2 maps global scaling is computed from the values obtained in the CALIFA fibers as compared to the SDSS images apertures. The minimum value of the χ^2 map is used to obtain the best RA and DEC position for the centre of the PPak IFU with respect to the center of the CALIFA galaxy seen by SDSS. Fig. 8 shows an example of the described procedure. The photometric scale factor at the best matching position is used to rescale the absolute photometry of each particular RSS pointing to bring them on the same flux scale. However, in a few datacubes, this method gives not the best results, particularly in low surface brightness edge-on galaxies and bright foreground field stars. This effect is more likely to occur in the V1200 setup, because its average lower S/N compared to V500. When the new registration fails, we use the photometric SDSS matching of pipeline v1.3c described in

H13. For the sake of consistency, we apply the same registering method in both setups. The absolute astrometry of the v1.3c is less accurate than the new one, as well as photometry anchoring with the SDSS images. To easily identify the galaxies were the new registration method fails, we have included the keyword REGISTER in the header of the datacubes (see Sect. 4.4) and added a dagger symbol in the quality tables (Table 6 and 7).

The third step in the reduction sequence is the interpolation method used to convert from RSS to cube format, aimed to improve the spatial resolution. The best position for each RSS pointing obtained in the previous is used in the reconstruction of the image. Several test using the drizzle method (Fruchter & Hook 2002) and inverse-distance weighted image reconstruction scheme were carried out, favoring the last method. In order to increase the spatial resolution and reduce the correlation between nearby pixels, we have reduced the radius and dispersion of the Gaussian. The final values are 0.75″ for the dispersion (instead of 1″ in v1.3c) and a limit in radius of 3.5″ (instead of 5″). This results in a much sharp image and a lower value for the correlated noise. In previous the previous pipeline v1.3c, a minimum number of 3 fibers was imposed in the reconstruction of the image to achieve a homogeneous data quality across the field. Combined with the previous radius limit, however, for pipeline v1.5 this results in the absence of data in the outer 2″ of the FoV, due to the wider separation of fibers in the outer ring of the fiber bundle. Thus, we decided to lower this limit to 1 as the minimum number of fibers needed to fill a spaxels. We have added a new HDU to the datacube (see Sect. 4.3) containing the information of he number of fibers used to compute the flux of a particular spaxel. This allows the user to control what spaxels to include if a particular science case requires a minimum number of fibers for the reconstruction of the flux.

3.2. Characterization of spatially correlated noise

Due to the interpolation procedure to obtain a regular grid, the output pixels in the final datacube are not independent of one another. The gaussian interpolation method divides the flux from a given fiber between several pixels and combines them with neighbour ones up to a radius limit, as described in Sect. 3.1. This causes the noise in the adjacent pixels to be correlated (in the spatial dimension). The correlation implies that a measurement of the noise in a stacked spectra of N pixels will be underestimated (noise is underestimated on scales larger that pixel units). Characterizing this effect is essential for estimating the statistical errors when spectra in datacubes are co-added to increase the S/N, an regular approach in specific applications when a minimum S/N is required.

First, we check that the error spectra derived from the pipeline for individual spaxels are reliable. Spectral fitting analysis can provide an approximate assessment of the accuracy of the error spectra. In Fig. 9 we update Fig. 9 of H13 to DR2 data. The plot shows the histogram of reduced residuals, ie. the difference between the observed and synthetic spectra obtained with STARLIGHT in units of the corresponding error (details on the fitting procedures can be found in). The distribution is very well described by a gaussian centered at 0.03 and with $\sigma = 0.87$, only slightly less than expected on the assumption that residuals are purely due to noise.

The correlated noise can be taken into account by providing the spatial covariance (Sharp et al. 2014). However, a more practical approach consist of using the datacubes to calculate the expected r.m.s noise. with the noise correlation ratio $\beta(N)$, as a function of the number of pixels. To obtain a sample of co-added

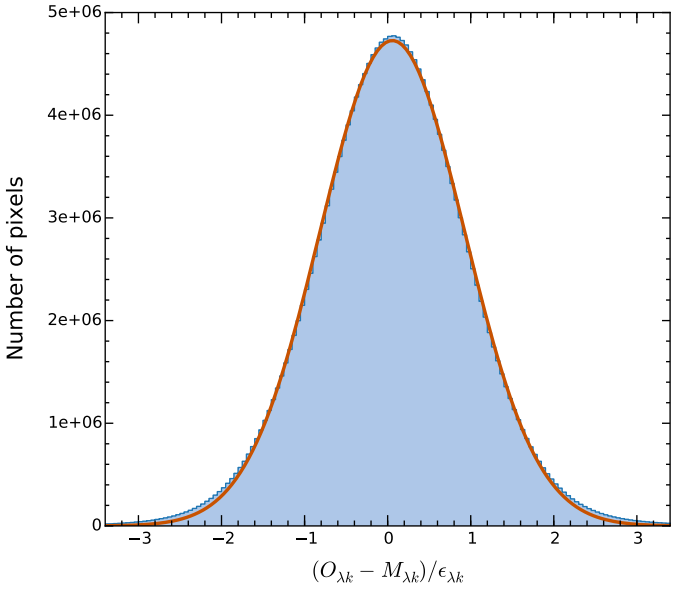

Fig. 9. Histogram of the reduced residuals $(O_{\lambda,k} - M_{\lambda,k})/\epsilon_{\lambda,k}$ for all λ's, all zones and all galaxies in DR2 (209151086 points in total). The solid orange line shows the best gaussian fit to the sample.

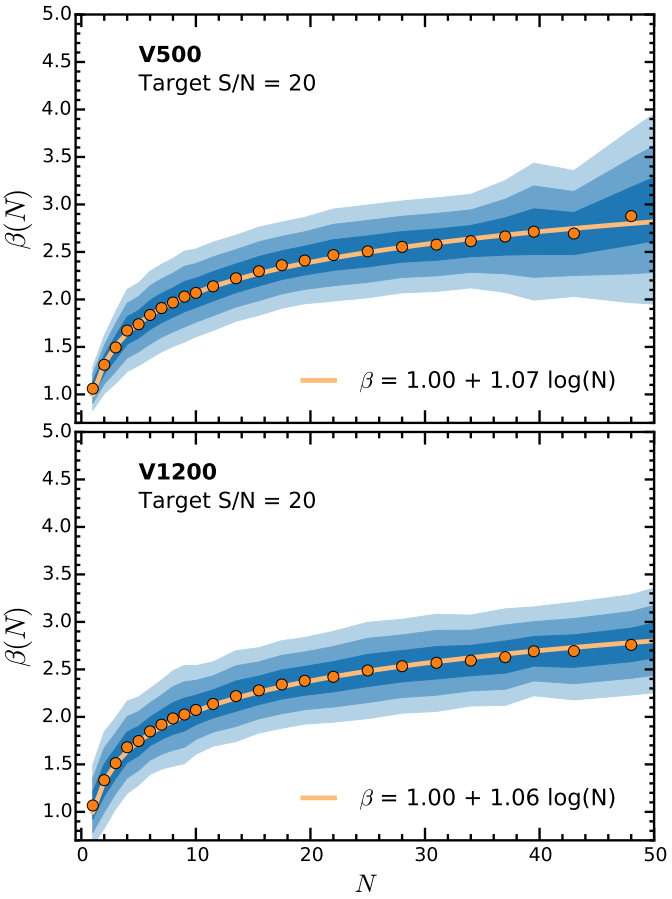

Fig. 10. Noise correlation ratio β (ratio of the real estimated error to the analytically propagated error) as a function of number of spaxels per bin for all the V500 (upper panel) and V1200 (lower panel) data of DR2 at a target S/N of 20. Shades areas mark the 1σ, 2σ and 3σ levels. The orange lines represent the best fit logarithmic function with a slope $\alpha = 1.07$ and $\alpha = 1.06$, respectively.

spaxels with different areas, we have used the Voronoi adaptive binning method (implemented for optical IFS data by Cappellari & Copin 2003) with a target S/N of 20. We have removed from the analysis individual spaxels with S/N < 5 and co-added bins with areas larger than 60 spaxels. The β correlation ratio (or correction factor) is no other but the ratio between the "real" or measured error to the analytically propagated error of the binned spectra as a function of bin size. The results obtained for all DR2 datacubes are shown in Fig. 10. This function can be described by a logarithmic function

$$\beta(N) = 1 + \alpha \log N, \quad (1)$$

with N the number of spaxels per bin.

The values for the slope α are equal within the errors (0.01) in both setups, with a value of 1.06 for V1200 and 1.07 for V500. The slope is lower than the DR1 value (mean ~ 1.4), indicating that the noise in DR2 datacubes is less correlated than in DR1. This is totally expected since we changed the parameters in the interpolation (reducing the number of adjacent fibers contribution to a particular spaxel) and the registering method. In Appendix A we give some instructions on how to estimate the final co-added error spectrum and the limit of the application of equation 1.

4. CALIFA data format and characteristics

The CALIFA data are stored and distributed as datacubes (three-dimensional data) in the standard binary FITS format and consist of several FITS Header/Data units (HDU). These datacubes contain (1) the measured flux densities, corrected for Galactic extinction as described in S12, in units of 10^{-16} erg s^{-1} cm^{-2} Å^{-1} (primary datacube), (2) associated errors, (3) error weighting factors, (4) bad pixels flags and (5) fiber coverage (Table 2). The last HDU is a new added content absent in DR1, as explained in Sect. 3.1, but the rest of them share the same properties as the previous data release. The first two axes of the cubes correspond to the spatial dimension along right ascension and declination with a $1'' \times 1''$ sampling. The third dimension represents the wavelength along a linear grid. Table 3 summarizes the dimensions of each datacube (N_α, N_δ, and N_λ), as well as the spectral sampling (d_λ) and constant resolution (δ_λ) along the entire wavelength range.

4.1. Error and weight datacubes

The errors associated 1σ noise level of each pixel as formally propagated by the pipeline can be found in the first FITS extension. Sect. 3.2 discusses on the accuracy of the formal noise and the correlation, important when CALIFA data need to be spatially binned, and an empirical function is provided to account for the correlation effect. The second FITS extension (ERRWEIGHT) stores the error scaling factor for each pixel in the limiting case that all valid spaxels of the cube would be co-added (see also Appendix A). In the case of bad pixels, we assigned an error value that is roughly ten orders of magnitude higher than the typical value.

4.2. Bad pixel datacubes

Bad pixel datacubes are stored in the third FITS extension (BADPIX). This information, in combination with the error vector, is essential to properly account for the potential problems en each spaxels in any analysis. Pixels with flag = 1 reports absence of sufficient information in the raw data due to cosmic rays, bad CCD colums or the effect of vignetting[3]. These bad pixels have been interpolated and we strongly suggest not to use them for any science analysis.

Finally, the uncovered corners of the hexagonal PPak FoV are filled with zeros and flagged as bad pixels for consistency. The residuals of bright night-sky emission lines are not flagged as bad pixels.

Table 3. Dimension and sampling of CALIFA datacubes

Setup	N_α [a]	N_δ [a]	N_λ [a]	λ_{start} [b]	λ_{end} [c]	d_λ [d]	δ_λ [e]
V500	78	73	1877	3749Å	7501Å	2.0Å	6.0Å
V1200	78	73	1701	3650Å	4840Å	0.7Å	2.3Å

Notes. [(a)] Number of pixels in each dimension. [(b)] Wavelength of the first pixel on the wavelength direction. [(c)] Wavelength of the last pixel on the wavelength direction. [(d)] Wavelength sampling per pixel. [(e)] Homogenized spectral resolution (FWHM) over the entire wavelength range.

4.3. Fiber coverage datacubes

Pipeline V1.5 adds a new FITS extension (FIBCOVER) to the datacubes, not available in previous DR1 datacubes. As explained in Sect. 3.1 we have reduced the radius limit of fibers that can account to the flux of a particular spaxel. The outer hexagonal-ring of fibers do not have the same coverage in the surroundings as any other fiber inside the hexagon. In pipeline V1.3c we imposed a minimum of 3 fibers for computing the flux of given spaxel. In V1.5, with the new radius limit this would yield an empty outer hexagonal-ring of ~ 2″in the FoV. Thus, we have relaxed to 1 the minimum number of fibers. In order to control control which spaxels have enough flux "resolution", we have included a new HDU reporting the number of fibers used to account for the computed flux.

4.4. FITS header information

The FITS header contains the standard keywords that register the spatial information according to the World Coordinate System (WCS, Greisen & Calabretta 2002) and the wavelength to the spectral axis in a linear grid. Each CALIFA datacube contains the full FITS header information of all raw frames from which it was created. Information regarding observing and instrumental conditions like for example sky brightness, flexure offsets, Galactic extinction or approximate limiting magnitude is also kept in the FITS header of each datacube. See Sect. 4.3 of H13 for nomenclature and their Table 4 for a summary of the main header keywords and meaning.

The most important new keyword added in DR2 datacubes is "REGISTER" and takes a boolean value. It indicates if a particular datacube has been successfully registered using the new method explained in Sect. 3.1 (*True*) or it has used the old V1.3c scheme (*False*). Datacubes with a *False* value are marked with a dagger in tables 4 and 5.

[3] The vignetting effect imprints a characteristic non homogeneous pattern across the FoV on the bad pixels vector. See Fig. 11 of H13 for more details.

Table 2. CALIFA FITS file structure

HDU	Extension name	Format	Content
0	Primary	32-bit float	flux density in units of 10^{-16} erg s^{-1} cm^{-2} Å^{-1}
1	ERROR	32-bit float	1σ error on the flux density
2	ERRWEIGHT	32-bit float	error weighting factor
3	BADPIX	8-bit integer	bad pixel flags (1=bad, 0=good)
4	FIBCOVER	8-bit integer	number of fibers used to fill each spaxel

5. Data Quality

This second CALIFA data release (DR2) provides science grade data for a sample of 200 galaxies, including the 100 galaxies released in the first data release (DR1). As for DR1, we have run a careful quality control (QC) on the data products and selected only those galaxies that passed a series of QC control checks in both setups (V500 and V1200), as we detail in this section. The QC checks are based on a set of measured parameters and/or visual inspection, resulting in a set of flags that allow to quickly assess the quality of the data and their suitability for scientific use. Quantities and flags are organized into three distinct categories, respectively related to: observing conditions (denoted by the OBS prefix); instrumental performance and effectiveness of the data reduction (RED); accuracy and quality of the final data products (CAL). The flags in each category are computed based on thresholds on measured quantities, possibly combined with flags given by human classifiers based on visual inspection, as detailed below and summarized in Tables 4 and 5. Thresholds are determined from the distribution of the parameters in order to exclude outliers and also by analyzing the effects of anomalous parameters on the final quality of the datacubes. We release the tables of the relevant QC parameters, along with the QC flags on the DR2 website.

Each flag can have one of the following values:

- -1 = undefined
- 0 = good quality – OK
- 1 = minor issues that do not significantly affect the quality – WARNING
- 2 = significant issues affecting the quality – BAD

By selection, DR2 only includes galaxies with WARNING flags in the worst cases, with just a few minor exceptions affecting previously released DR1 galaxies: in these cases the revised QC criteria adopted here would have prevented to include such galaxies in the DR, but given the incremental nature of our data releases we keep them in the current sample.

In naming the QC parameters we adopt the following convention: the first part is the category prefix (OBS, RED or CAL), followed by a measured parameter, and possibly a final suffix indicating the statistics applied to combine the parameter as measured in different observations/pointings/fibers (i.e., MEAN, MIN, MAX, RMS).

In the following subsections we describe the QCs in each of the above-mentioned categories. As mentioned in Sect. 3.1, V1.5 pipeline starts after sky subtraction of the individual RSS files. Thus, some of the quality and properties of the DR2 datacubes are inherited from DR1 and will not be discussed here namely, wavelength calibration and sky subtraction.

5.1. Quality of the observing conditions (OBS)

Three quantities are considered crucial in determining the quality of the observing conditions of the CALIFA data: the airmass, the brightness of the sky, and the atmospheric extinction. While seeing is in general an important parameter of the observing conditions, the imaging quality and spatial resolution of the CALIFA cubes is mostly limited by the sampling of the fibers on the plane of the sky and the resampling process (see section 5.4.1 for more detail), rather than by the natural seeing. Moreover, the seeing measurement is only available for a small fraction of the objects, and therefore cannot be used as a reliable QC parameter.

For the airmass we consider the average and the maximum airmass of the observations over all pointings (OBS_AIRMASS_MEAN and OBS_AIRMASS_MAX) and its rms (OBS_AIRMASS_RMS). For each of these quantities we defined two thresholds (same for V500 and V1200, see table 6 and 7) above which the WARNING or the BAD flags, respectively, are raised. The combined FLAG_OBS_AM is the worst of the three cases.

The surface brightness of the sky in V-band during the observations is another critical parameter, which mainly limits the depth of the observations and the accuracy of the sky subtraction. This quantity SKYMAG is measured in each pointing from the sky spectrum obtained from the 36 sky fibers[4]. The mean and the rms over all pointings are considered to define the corresponding flags. Note that stricter requirements are applied to V1200 data (blue setup, high resolution) with respect to the V500 ones.

The transparency of the sky during each pointing (EXT) is obtained from the monitored V band extinction at the time of the observation. We consider as symptoms of low/bad quality observations large extinctions on average, a large maximum extinction or a large rms variation across the pointings (indicating inhomogeneous observing conditions).

5.2. Quality of the instrumental/data reduction performance (RED)

The quality of the instrumental and data reduction performance is assessed via a series of four quantities measured on the reduced data *before* combining them into the final datacube: STRAYLIGHT, spectral DISPERSION, cross dispersion CDISP, and the residuals from the subtraction of bright skylines (namely, the 5577Å O_2 line in the V500 setup and the 4358Å HgI in the V1200 setup). In addition we consider the limiting surface brightness corresponding to a 3-σ detection measured on the final cube.

The so-called straylight is effectively a background source of illumination: its origin is not completely clear as far as PPAK-PMAS is concerned, although it most likely arises from the electronics of the camera[5]. The higher the straylight, the lower is the final sensitivity and accuracy of the data reduction steps. High mean level of straylight in a frame (MEANSTRAYLIGHT), as well as high maximum values (MAXSTRAYLIGHT) and large rms (RMSSTRAYLIGHT), are indication of poor performance. Lev-

[4] See Appendix A.8 of H13.

[5] For a detailed description on the straylight subtraction, see Appendix A.3 of H13.

Table 4. Definition of CALIFA DR2 quality control flags for the V500 data

QC flag	QC parameters involved	WARNING condition(s)	BAD condition(s)	Flag definition
FLAG_OBS_AM	OBS_AIRMASS_MEAN	> 1.7	> 2.0	Worst of the three parameters
	OBS_AIRMASS_MAX	> 2.0	> 2.5	
	OBS_AIRMASS_RMS	> 0.15	...	
FLAG_OBS_SKYMAG	OBS_SKYMAG_MEAN	< 20.5 mag_V $arcsec^{-2}$	< 19.5	Worst of the two parameters
	OBS_SKYMAG_RMS	> 0.1	...	
FLAG_OBS_EXT	OBS_EXT_MEAN	> 0.30 mag	...	Worst of the three parameters
	OBS_EXT_MAX	> 0.35	...	
	OBS_EXT_RMS	> 0.10	...	
FLAG_RED_STRAYLIGHT	RED_MEANSTRAYLIGHT_MAX	> 30 counts	> 50	Worst of the three parameters
	RED_MAXSTRAYLIGHT_MAX	> 50	> 100	
	RED_RMSSTRAYLIGHT_MAX	> 5	> 10	
FLAG_RED_DISP	RED_DISP_MEAN	> 5.5 Å (FWHM)	...	Worst of the three parameters
	RED_DISP_MAX	> 10.0	...	
	RED_DISP_RMS	> 0.5	> 1.0	
FLAG_RED_CDISP	RED_CDISP_MEAN	> 3.0 pixels (FWHM)	...	Worst of the three parameters
	RED_CDISP_MAX	≥ 4.0	...	
	RED_CDISP_RMS	> 0.25	...	
FLAG_RED_SKYLINES	RED_RES5577_MIN	< −0.1 counts	...	Worst of the three parameters
	RED_RES5577_MAX	> 0.1	...	
	RED_RMSRES5577_MAX	> 1.0	...	
FLAG_RED_LIMSB	RED_LIMSB	< 23.25 mag_V $arcsec^{-2}$	< 22.50	
FLAG_CAL_SPECPHOTO	CAL_QFLUX_G	> 0.06 dex	> 0.097 dex	Worst of the three parameters
		< −0.06 dex	< −0.097 dex	combined with visual checks
	CAL_QFLUX_R	> 0.06 dex	> 0.097 dex	on the 30"-integrated spectrum:
		< −0.06 dex	< −0.097 dex	spectral shape and comparison
	CAL_QFLUX_RMS	> 0.1	> 0.2	with SDSS photometry
FLAG_CAL_WL	CAL_RMSVELMEAN	> 2.0 km s^{-1}	> 5.0	
FLAG_CAL_IMA	CAL_CHI2REG_MAX	> 10	...	Combine parameter and visual inspection on registration and synthetic broad-band image

els above the thresholds provided in tables 4 and 5 in at least one of the exposures (_MAX suffix) raise a WARNING or a BAD FLAG_RED_STRAYLIGHT flag.

The spectral dispersion and cross dispersion are measured on individual fiber spectra as the FWHM of skylines and the FWHM of the spectral trace, respectively. Thresholds are set on the mean values to ensure that the typical parameters do not depart too much from the nominal target specifications, and on the maximum and rms in order to check for anomalies in the data. Any failure to comply within the thresholds reported in tables 4 and 5 raises a FLAG_RED_DISP or FLAG_RED_CDISP.

In order to assess the performance of the sky subtraction we consider the minimum and the maximum over all pointings of the average (over all fibers) flux residual of a bright skyline within an individual pointing (RED_RES4358_MIN and RED_RES4358_MAX, and RED_RES5577_MIN and RED_RES5577_MAX for the V1200 and the V500 setup respectively). We also consider the maximum over all pointings of the rms residuals (over all fibers in an individual pointing), RED_RMSRES4358_MAX and RED_RMSRES5577_MAX. Too negative or too positive average residuals, are indication of systematic bias in the sky subtraction. Too large an rms can be regarded as symptom of localized failures or noisy data. In these cases the FLAF_RED_SKYLINES is set.

Finally, the 3σ continuum flux density detection limit per interpolated 1 $arcsec^2$ - spaxel for the faintest regions is used to identify cubes whose depth does not fulfil the survey requirements and this is reflected in the FLAG_RED_LIMSB flag. More about the depth of the final datacubes is shown and discussed in Sec. 5.6.

Table 5. Definition of CALIFA DR2 quality control flags for the V1200 data

QC flag	QC parameters involved	WARNING condition(s)	BAD condition(s)	Flag definition
FLAG_OBS_AM	OBS_AIRMASS_MEAN	> 1.7	> 2.0	Worst of the three parameters
	OBS_AIRMASS_MAX	> 2.0	> 2.5	
	OBS_AIRMASS_RMS	> 0.15	...	
FLAG_OBS_SKYMAG	OBS_SKYMAG_MEAN	$< 21.5\ \mathrm{mag_V\ arcsec^{-2}}$	< 21.0	Worst of the two parameters
	OBS_SKYMAG_RMS	> 0.1	...	
FLAG_OBS_EXT	OBS_EXT_MEAN	> 0.30 mag	...	Worst of the three parameters
	OBS_EXT_MAX	> 0.35	...	
	OBS_EXT_RMS	> 0.10	...	
FLAG_RED_STRAYLIGHT	RED_MEANSTRAYLIGHT_MAX	> 15 counts	> 30	Worst of the three parameters
	RED_MAXSTRAYLIGHT_MAX	> 20	> 40	
	RED_RMSSTRAYLIGHT_MAX	> 1.5	> 2.0	
FLAG_RED_DISP	RED_DISP_MEAN	> 2.0 Å (FWHM)	> 2.5	Worst of the three parameters
	RED_DISP_MAX	> 10.0	...	
	RED_DISP_RMS	> 0.15	...	
FLAG_RED_CDISP	RED_CDISP_MEAN	> 3.0 pixels (FWHM)	...	Worst of the two parameters
	RED_CDISP_RMS	> 0.66	...	
FLAG_RED_SKYLINES	RED_RES4358_MIN	< −0.1 counts	...	Worst of the three parameters
	RED_RES4358_MAX	> 0.1	...	
	RED_RMSRES4358_MAX	> 0.7	...	
FLAG_RED_LIMSB	RED_LIMSB	$< 22.50\ \mathrm{mag_B\ arcsec^{-2}}$	< 22.00	
FLAG_CAL_SPECPHOTO				Visual checks on 30"-aperture integrated spectrum for spectral shape and mismatch with V500 spectrophotometry
FLAG_CAL_WL	CAL_RMSVELMEAN	$> 1.0\ \mathrm{km\ s^{-1}}$	> 2.0	
FLAG_CAL_IMA	CAL_CHI2REG_MAX	> 10	...	Combine parameter and visual inspection on registration and synthetic broad-band image

5.3. Quality of the calibrated data products (CAL)

The quality of the calibrated data products is determined by checks on the global spectrophotometry, on the stability of the wavelength calibration across the spectral range, and on the quality of the resulting 2D flux distribution (synthetic image) and its ability to match the SDSS broad-band imaging.

The quality of global spectrophotometric calibration is assessed by comparing the photometric fluxes derived from spectra integrated within 30″-radius apertures with the corresponding fluxes derived from SDSS imaging, as explained below in Sec. 5.5. For the V500 setup, in particular, it is possible to derive the flux ratio between SDSS and CALIFA in *g* and *r*-band (CAL_QFLUX_G and CAL_QFLUX_R, respectively, averaged over all pointings for a given galaxy): values of these ratios departing from 1 more than the tolerances listed in table 4 are flagged. Large rms variations of these values over the three V500 pointings (CAL_QFLUX_RMS, which combines *g* and *r* bands) are also considered symptoms of poor quality. In addition to these quantitative parameters, we perform visual checks that the spectral energy distribution (SED) measured via SDSS photometry matches the CALIFA integrated spectrum. For this check we also consider the *u* and the *i* band data-points: although the CALIFA spectra do not cover the full extent of these pass-bands, they prove helpful in judging the matching of spectral shapes. Five members of the collaboration have performed these checks independently and assigned flags OK-WARNING-BAD: the second-to-worst classification is retained. This flag is then combined with the flags based on the quantitative flux ratios to create the final FLAG_CAL_SPECPHOTO flag.

In order to check the stability of the wavelength calibration over the full the spectral range we performed the same measurements presented in Sec. 5.3 of DR1: for each galaxy and setup, the spectra within 5″from the center of the galaxy are integrated

and the systemic velocity is estimated first for the full spectrum and then for 3 (4) independent spectral ranges in V1200 (V500); the rms of these values with respect to the systemic velocity from the full spectrum (CAL_RMSVELMEAN) is an estimate of the stability of the wavelength calibration across the wavelength range and is used to set the corresponding quality flag FLAG_CAL_WL. In > 97.5% of the cases we obtain CAL_RMSVELMEAN well below 2 km sec^{-1} for the V1200 and 3 km sec^{-1} for the V500 grating.

Finally, the quality flag on the 2D flux distribution and plane-of-sky registration, FLAG_CAL_IMA, is defined by combining the information on the goodness of matching between SDSS images and synthetic images from the CALIFA datacube and a series of visual checks. The former piece of information is provided by the chi-squared of the registration procedure (see Sect. 3.1). The visual checks include: a check on possible artefacts in the synthetic broad band image from the final CALIFA cubes (e.g. mismatched features, elongated PSF); a comparison of the CALIFA fiber footprints of each pointing with the registered SDSS image, looking for apparent mismatched and miscomputed spatial offsets; a check of the surface plot displaying the dependence of the registration procedure (see below) on the x and y spatial offsets, whereby irregular chi-square surfaces and lacks of clear minimum likely imply the impossibility of an accurate registration. Out of five independent classifiers we chose the median value of the attributed flags and combine it with the flag corresponding to the chi-squared measurements. Importantly, we note that a small number of objects already released as part of DR1 do not reach the imaging quality standards using the registration procedure adopted in the pipeline V1.5 (see Sect. 3.1), which uses cross-correlation with SDSS images: in these cases we revert to the old registration scheme adopted for DR1 (pipeline V1.3c) and mark the objects with a dagger in tables 4 and 5.

5.4. Astrometric accuracy and spatial resolution

5.4.1. Astrometric registration accuracy

5.4.2. Seeing and spatial resolution

In order to cover the complete FoV of the central bundle and to increase the final resolution of the CALIFA data cubes (PPak fibers have a diameter of 2.7″), a dithering scheme with three pointings has been adopted as described in S12. In imaging, in addition to the telescope aperture, instrumental and atmospheric seeing determine the final spatial resolution. This has to be added to the IFU particular characteristics.

Seeing in the CALIFA data was measured from the differential image motion monitor (DIMM, Aceituno 2004), which operates fully automatically at the Calar Alto observatory during the night. DIMM has certain operational constraints (humidity lower than 80% and wind speed less than 12 m s^{-1}) than the 3.5m telescope, thus seeing information is not available for every CALIFA observation. Thus, there can be some DIMM seeing missing from Tables 6 and 7, but the overall seeing distribution is not expected to be very different. Fig. 11 shows the DIMM seeing for the DR2 sample, with and has a median value of 0.″9 (FWHM) (the distribution is very similar to the DR1 sample), and therefore atmospheric seeing is not a limiting factor in the spatial resolution of the CALIFA cubes.

Another improvement of the pipeline, as discussed 3.1, is the spatial resolution. Fig. 12 shows Hα maps (obtained using FIT3D) for NGC 5406 (ID 684) for DR1, DR2 and one image taken with the William Herschel Telescope (WHT). The last image has been also degraded to the DR2 nominal resolution for the

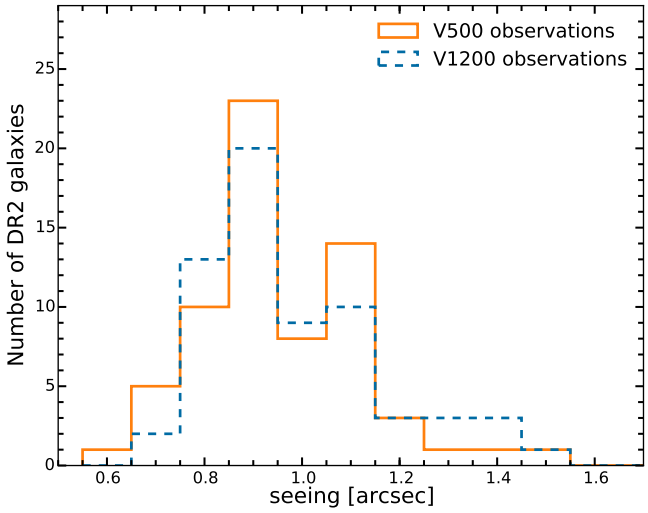

Fig. 11. Distribution of the seeing during the CALIFA observations as measured by the automatic Differential Image Motion Monitor (DIMM, Aceituno 2004).

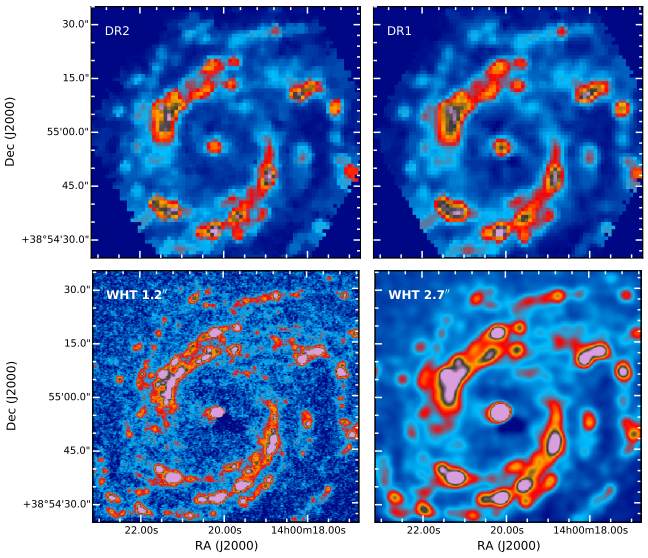

Fig. 12. DR2 spatial resolution comparison for NGC 5406 (ID 684). The upper left panel shows the DR2 image of the Hα map and the upper right the DR1 one. The lower row are Hα images taken with the 4.2m William Herschel Telescope (Roque de los Muchachos Observatory, La Palma, Spain), using the AUXCAM detector (Sánchez-Menguiano et al., in prep.). The image, with an original resolution of 1.2″(bottom left), has been degraded to a resolution of 2.6″(bottom right) and the FoV has been reduced to match exactly the same WCS coordinates as CALIFA.

sake of comparison. This improvement translates directly, for example, in a higher number of H II regions detected in DR2. Using HIIEXPLORER (Sánchez et al. 2012b) on the v1.3c datacubes of the 200 galaxies, a total of 5878 are recovered, while this number rises to 7646 H II regions for the DR2 galaxies using pipeline V1.5, which represents an increase of ∼ 30%.

We follow two different approaches to measure the PSF in the data cubes. In those cases when a bright foreground star is present not far from the center, a fit is performed to the radial distribution of the star light profile. When the PSF is good, the Moffat function fits better than the Gauss, as seen in Fig. 13.

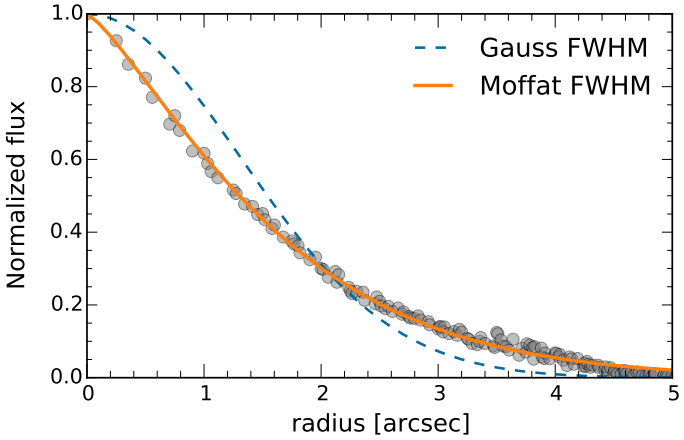

Fig. 13. Profile fit to a foreground star close to the center in the data cube of the galaxy NGC 2916. When the PSF is good, the Moffat function fits better than the Gauss.

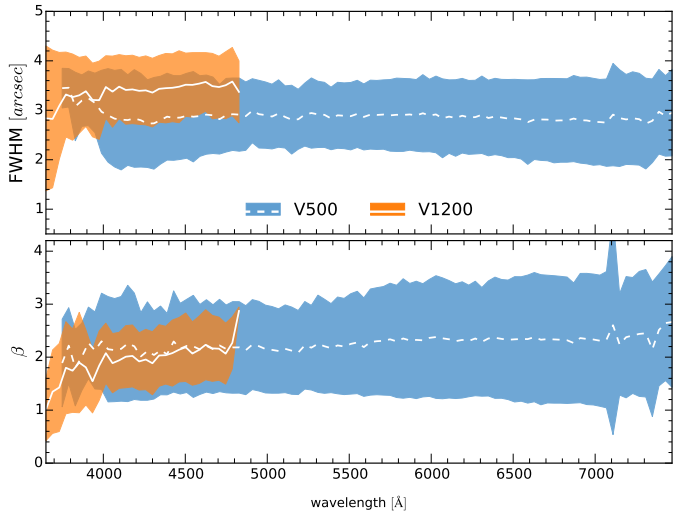

Fig. 14. Fitted PSF parameters as functions of wavelength. The top and bottom panels show the FHWM and β parameters of a 2-D Moffat profile. The filled area shows the $\pm 1\sigma$ range for the fitted parameters (blue for V500 and in orange for the V1200 setup). The white lines correspond to the mean values (V500 dashed, V1200 solid).

Both functions fit equally well when the PSF degrades. We investigate how the PSF behaves as a function of wavelength. The spectra are then resampled to bins of 40 Å, to get a better signal to noise and avoid interference of atmospheric and emission lines. To remove the galaxy background we mask the star and compute the radial profile of the light of the galaxy, then fill the masked pixels with the expected value in their positions. The background is subtracted from the star, which is then fitted to a 2-D Moffat profile using IMFIT (Erwin 2014)[6]. This procedure is applied to every wavelength, for 9 galaxies observed with V500 setup and 5 galaxies with V1200. Fig. 14 shows the mean values of the FWHM and β parameters of the Moffat profile as functions of wavelength, for both setups. There is no wavelength dependence in any parameter. The mean values of FWHM are 2.9 ± 0.8 arcsec (V500) and 3.4 ± 0.8 arcsec (V1200), and the mean β are 2.3 ± 1.0 (V500) and 1.9 ± 0.7 (V1200). The ellipticity of the Moffat profile is 0.2 ± 0.1 in both setups. These uncertainties correspond to 1-σ of the distributions.

[6] http://www.mpe.mpg.de/~erwin/code/imfit/

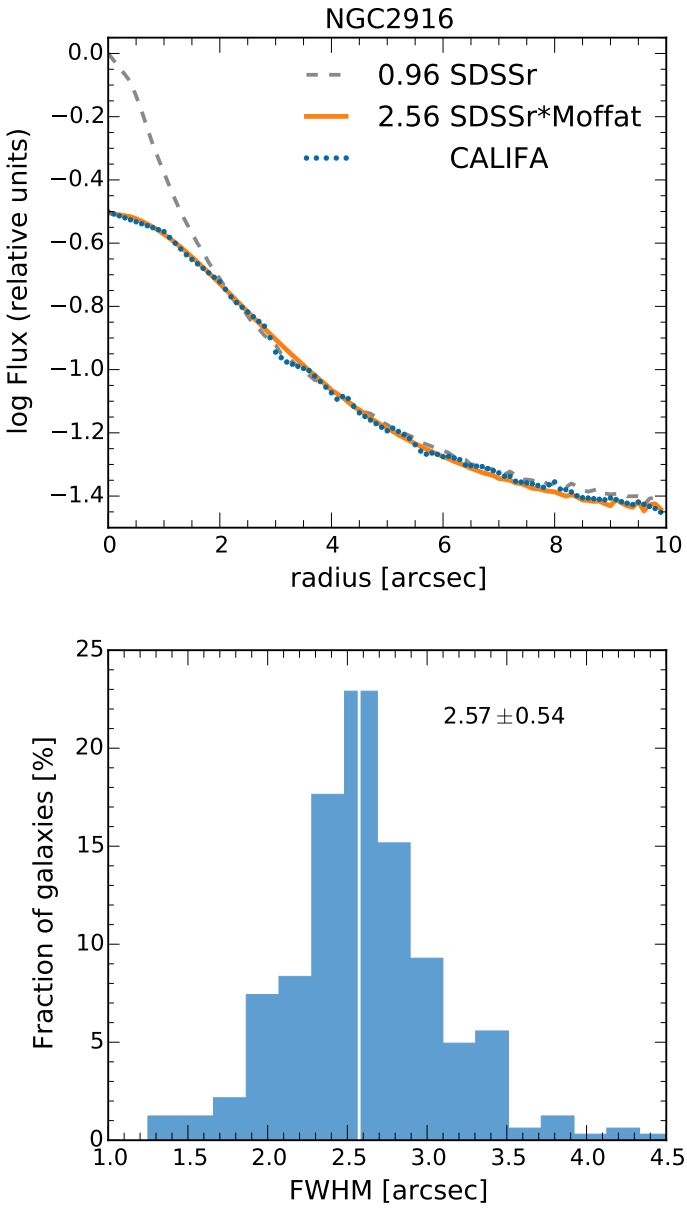

Fig. 15. *Upper panel:* The dashed (grey) line is the flux profile of the galaxy NGC 2916 from the original SDSS r band image, with a PSF FWHM = 0.″96 (as obtained from the SDSS Skyserver), the dotted (blue) line is the flux profile from the CALIFA data cube of NGC 2916, and the continuous (blue) line is the profile from the convolution of the SDSS r image a 2D Moffat kernel of width 2.″37, resulting in a final PSF FWHM = 2.″56. *Bottom panel:* Distribution of FWHM obtained for all galaxies for the case of convolving SDSS r images with a Moffat kernel, with values around 2.57 ± 0.54 arcsec (white line).

The method can be applied only to a few galaxies, so we follow a second method that can be applied to all the data cubes. The second method is based on the fact that the nuclei of galaxies have a relatively steep luminosity profile, and we take advantage of the good quality of the SDSS images. For each galaxy, the SDSSS r band image is convolved with a 2D function (Moffat or Gauss) and we compute the residuals after subtracting the resulting flux radial distribution from the flux radial distribution of the data cube of the same galaxy. A range of FWHM for the convolution function are used and we choose the one that minimizes the residuals. An example for the galaxy NGC 2916 is

shown in the central panel of Fig. 15 for the case of convolving with a Moffat kernel. The dashed (grey) line is the flux profile of the original SDSS r band image, with a PSF FWHM = 0.″96 (as obtained from the SDSS Skyserver), the dotted (blue) line is the flux profile from the CALIFA data cube, and the continuous (orange) line is the convolution of the black profile with a 2D Moffat kernel of width 2.″37, resulting in a final PSF FWHM = 2.″56. *Bottom panel* of Fig. 15 shows the distribution of FWHM obtained for all galaxies for the case of convolving with a Moffat kernel, with values around 2.57 ± 0.54 arcsec (white line).

5.5. Spectrophotometric accuracy

As mentioned in Sect. 3.1 the new registration scheme of the pipeline uses SDSS *r* band for the V500 setup and *g* band for the V1200, and field calibration images of the SDSS DR7. Each V500 datacube is rescaled in the absolute flux level to match the SDSS DR7 broad-band photometry using the photometric scale factor at the best matching position for each pointing. On the other hand, the V1200 data is matched to the V500 data (S12). This procedure, together with the new re-calibrated sensitivity curve (see Sect. 3.1 and Husemann et al., in preparation), improves the spectrophotometric calibration of DR1. This is clearly shown in Fig. 16. As part of the CALIFA pipeline V1.5, an 30″diameter photometric aperture in *r* and *g* is measured both in the SDSS DR7 images and the equivalent synthetic CALIFA broad-band images. The mean SDSS/CALIFA *g* and *r* band ratios in DR2 are 1.00 ± 0.05 and 0.99 ± 0.06, respectively. In the *right panel* of Fig. 16 the distribution in $\Delta(g-r)$ color difference between the SDSS and CALIFA data shows that the spectrophotometric accuracy across the wavelength range is better that 3%, with a median value of 0.01 ± 0.03.

Spectral fitting methods can be used to perform useful tests of the data and their calibration, and this has been done before in CALIFA. H13 used STARLIGHT fits to evaluate the accuracy of the error estimates in DR1 datacubes, while Cid Fernandes et al. (2014) used such fits to map systematic features in the spectral residuals which may indicate calibration issues.

We have repeated these same experiments for the DR2 datacubes. Results are shown in Fig. 17. The top panel shows in black the mean spectrum of 170670 Voronoi zones of the 200 galaxies in DR2[7]. The averaging is done after normalizing each spectrum by it median flux in the 5635 ± 45 Å. The mean synthetic spectrum (overplotted orange line) as well the mean residual (at the bottom of the upper panel, purple line) are also plotted. The middle panel zooms in on the residual spectrum, which now excludes emission lines and bad-pixels masked away in the fitting process. Finally, the bottom panel show what fraction of all spectra was used in the statistics at each λ.

Fig. 17's layout is identical to Fig. 13 of Cid Fernandes et al. (2014), to which it should be compared[8]. Focusing on the middle panel, one sees that from ∼ 5000 Å to the red the residuals are very similar, including the humps around 5800 Å, associated to imperfect removal of telluric features. Towards the blue, however, one sees that the new reduction pipeline leads to smaller residuals. For instance, the broad through around Hβ seen with v1.3c spectra is essentially gone with the new reduction. A systematic excess blueness persists for $\lambda < 3900$ Å, but overall the improvement is clear.

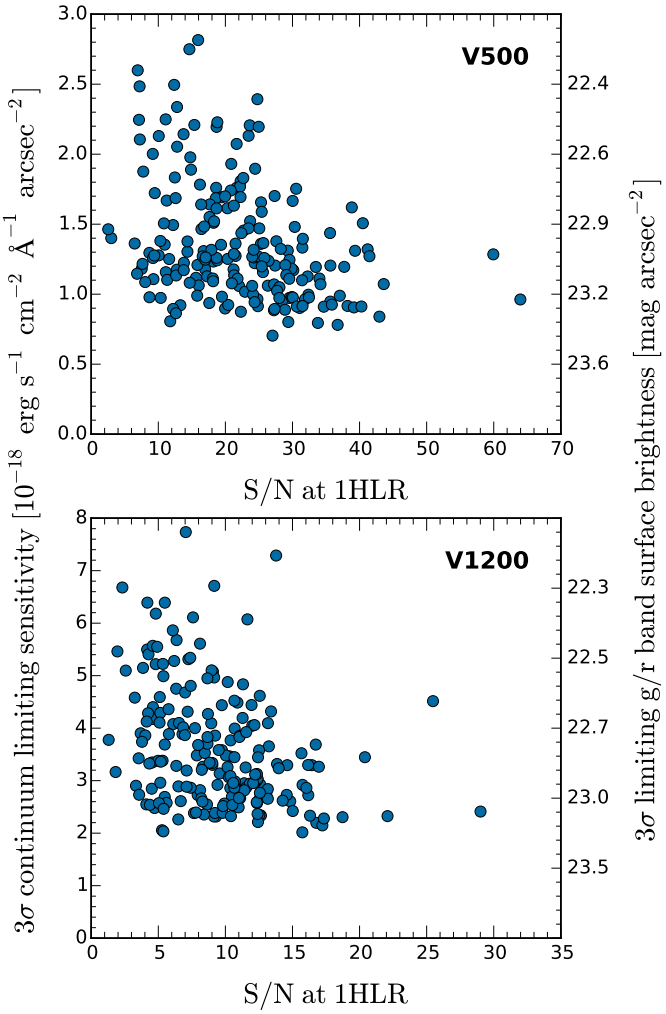

Fig. 19. Limiting 3σ continuum sensitivity as a function of the average continuum S/N at the half light radius (HLR). The corresponding broad-band surface brightness limits in *r* (V500) and *g* (V1200) are indicated on the right *y*-axis. The limiting continuum sensitivity and the S/N were computed from the median signal and noise in the wavelength region 4480–4520Å and 5590–5680Å for the V1200 and V500 data, respectively.

Residuals for the 200 DR2 nuclear spectra are shown in Fig. 18, where galaxies are sorted by redshift and piled up. This visualization facilitates the identification of telluric features, which appear as slanted lines in the image. Comparison with an identical plot in H13 (their Fig. 16) shows the improvements achieved with the new pipeline.

5.6. Limiting sensitivity and signal-to-noise

In order to assess the depth of the data, we estimated the 3σ continuum flux density detection limit per interpolated 1 arcsec^2-spaxel for the faintest regions. Fig. 19 shows the limiting continuum sensitivity of the spectrophotometrically recalibrated SDSS spectra. The depth is plotted against the average S/N per spectral resolution element within in an elliptical annulus of ±1″ around the galaxies *r* band half-light semi-major axis (HLR), with PA

[7] The spatial binning is used to guarantee a minimum S/N of 20 in the continuum at ∼ 5635 Å. In practice, 88% of the Voronoi zones actually comprise a single spaxel.

[8] Fig. 13 in Cid Fernandes et al. (2014) is in fact busier than our Fig. 17, as its shows results obtained with three different spectral bases. Here we adopt the same base described in González Delgado et al. (2014b), which is very similar to base *GM* in Cid Fernandes et al. (2014).

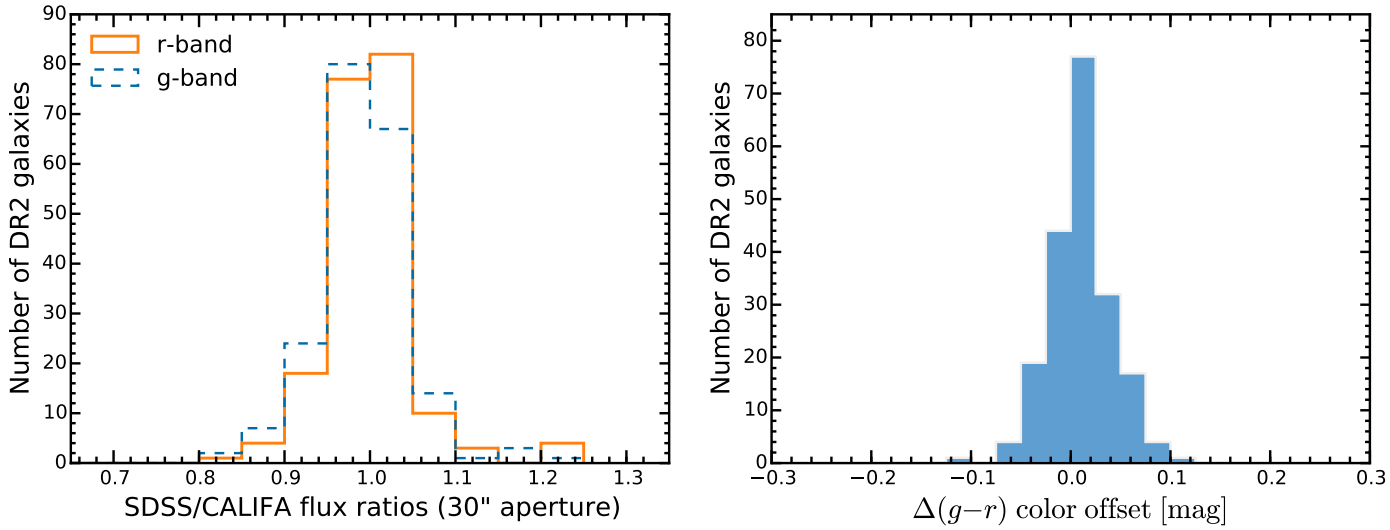

Fig. 16. *Left panel:* Distribution of the 30″ aperture photometry scale factor between the SDSS DR7 images and re-calibrated CALIFA data. We compare the photometry only for the *g* and *r* bands, which are both entirely covered by the V500 wavelength range. *Right panel:* Distribution of the corresponding color offset between the SDSS DR7 images and the synthetic CALIFA broad-band images.

and radius values taken from W14. A narrow wavelength window at 4480–4520Å for the V1200 and at 5590–5680Å for the V500 was used to estimate both values. These small windows are nearly free of stellar absorption features or emission lines. The 3σ continuum flux density detection limit[9] for the V1200 data ($I_{3\sigma} = 3.2 \times 10^{-18}$ erg s^{-1} cm^{-2} Å^{-1} arcsec^{-2} in the median at 4500Å) is a factor of ~2-3 brighter than for the V500 data ($I_{3\sigma} = 1.2 \times 10^{-18}$ erg s^{-1} cm^{-2} Å^{-1} arcsec^{-2} in the median at 5635Å) mainly due to the difference in spectral resolution. These continuum sensitivities can be transformed into equivalent limiting broad band surface brightnesses of 23.0 mag arcsec^{-2} in the *g* band for the V1200 data and 23.4 mag arcsec^{-2} in the *r* band for the V500. The variance of the sky brightness of each night might be on of the main factors of the dispersion in the limiting continuum sensitivity. Dust attenuation, transparency of the night, and other atmospheric conditions might also affect the achievable depth at fixed exposure times.

The limiting sensitivity is a measure of the noise and thus in correlates mildly with the S/N. The mean S/N in the continuum per spaxel at the half-light semi-major axis (HLR) of all objects is ~9.5 for the V1200 setup, while it is ~22.2 for the V500 data. Thus, we achieve a S/N$\gtrapprox$10 for a significant number of the objects even for the V1200 setup.

6. Access to the CALIFA DR2 data

6.1. The CALIFA DR2 search and retrieval tool

The public data is distributed through the CALIFA DR2 web page (http://califa.caha.es/DR2). A simple web form interface, already in use for the first data release, allows to select data of a particular target galaxy, or a subsample of objects within some constraints observing conditions or galaxy properties. Among the selection parameters we include the instrument setup, galaxy coordinates, redshift, *g* band magnitudes, observing date, Hubble type, bar strength, inclination estimated from axis ratio, V band atmospheric attenuation, airmass, and relative accuracy of the SDSS/CALIFA photometric calibration.

[9] Note that this is a continuum flux density. See Note 5 of H13.

If CALIFA datasets are available within the given constraints, they are listed in the succeeding web page to make a final selection for download. The download process requests a target directory on the local machine to store the data, after the downloading option was selected. The CALIFA data are delivered as fully reduced datacubes in FITS format separately for each of the two CALIFA spectral settings, i.e. the V500 and V1200 setup. Each DR2 dataset is uniquely identified by their file name, *GALNAME*`.V1200.rscube.fits.gz` and *GALNAME*`.V500.rscube.fits.gz` for the V1200 and V500 setup respectively, where *GALNAME* is the name of the CALIFA galaxy listed in 1.

6.2. Virtual Observatory services

CALIFA data can be accessed using the Virtual Observatory (VO) Table Access Protocol (TAP, Dowler et al. 2011) at the TAP URL http://dc.g-vo.org/tap (service ivo://org.gavo.dc/__system__/tap/run). We provide tables describing each cube as a single data product (califadr2.cubes **CHECK with Markus!!!**) including the QC parameters reported in Tables 6 and 7 as well as tables containing all fluxes of the entire DR2 by position and wavelength (califadr2.fluxv500 and califadr2.fluxv1200) for the two setups separately. The table schemata can be obtained using the usual TAP means and tables can be easily retrieved and queried through the VO client TOPCAT6. Example queries and links will be provided on the DR2 web page to guide the user. The cubes can also be found in the GAVO data center's ivoa.obscore tables with a complete ObsCore metadata set (Tody et al. 2011) and the corresponding links are also stored in the califadr2.cubes table. Individual spectra can also be accessed using IVOA's Simple Spectral Access Protocol using the service ivo://org.gavo.dc/califa/q/s. This allows for easy access from within analysis programs like Splat and an example will be provided on the DR2 web page. An overview of VO-accessible resources generated from CALIFA data is available at http://dc.g-vo.org/browse/califa/q.

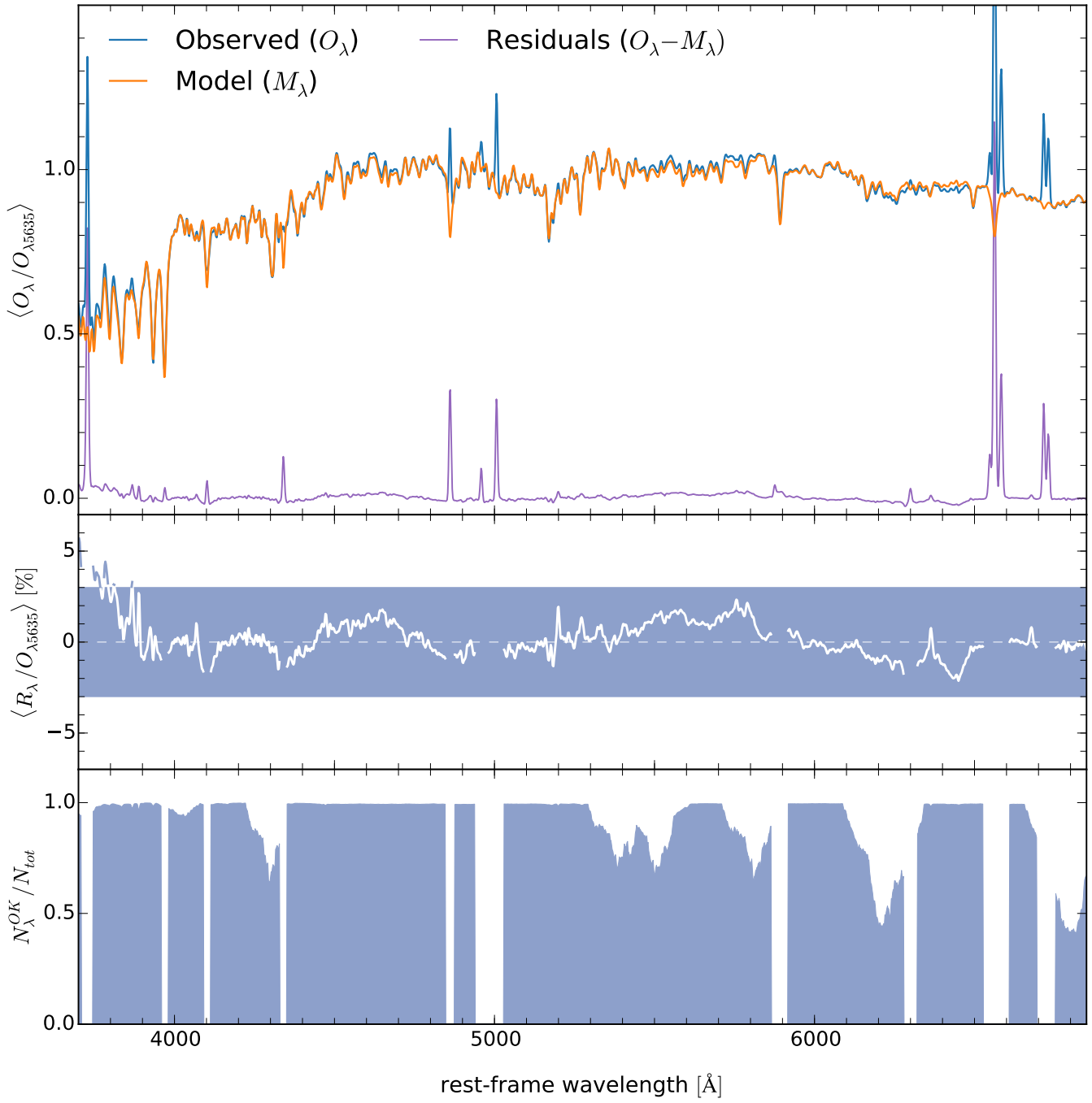

Fig. 17. Statistics of the spectral residuals (compare to Fig. 13 of Cid Fernandes et al. 2014). *Top:* The mean normalized spectrum of 170670 zones from 200 galaxies. The mean STARLIGHT fit is overplotted in orange, while the mean residual is plotted at the bottom of the panel (purple). *Middle:* Zoom of the residual spectrum, with emission lines removed for clarity. The shaded rectangle encompasses the ± 3% area. *Bottom:* Fraction of the zones contributing to the statistics at each λ.

7. Conclusions

We have shown that CALIFA is indeed an awesome survey.

In this article we describe the data distributed with the second public data release of the Calar Alto Legacy Integral Field Area (CALIFA) survey. The CALIFA DR2 provides science-grade and quality-checked integral-field spectroscopy data for 200 nearby galaxies publicly distributed to the community at http://califa.caha.es/DR2.

Acknowledgements. CALIFA is the first legacy survey being performed at Calar Alto. The CALIFA collaboration would like to thank the IAA-CSIC and MPIA-MPG as major partners of the observatory, and CAHA itself, for the unique access to telescope time and support in manpower and infrastructures. The CALIFA collaboration thanks also the CAHA staff for the dedication to this project. R.G.-B. has been supported by the Spanish *Ministerio de Ciencia e Innovación* under grant AYA2010-15081.

References

Abazajian, K. N., Adelman-McCarthy, J. K., Agüeros, M. A., et al. 2009, ApJS, 182, 543

Aceituno, J. 2004, Calar Alto Newsletter No. 8, http://www.caha.es/newsletter/news04b/Aceituno/Newsletter.html

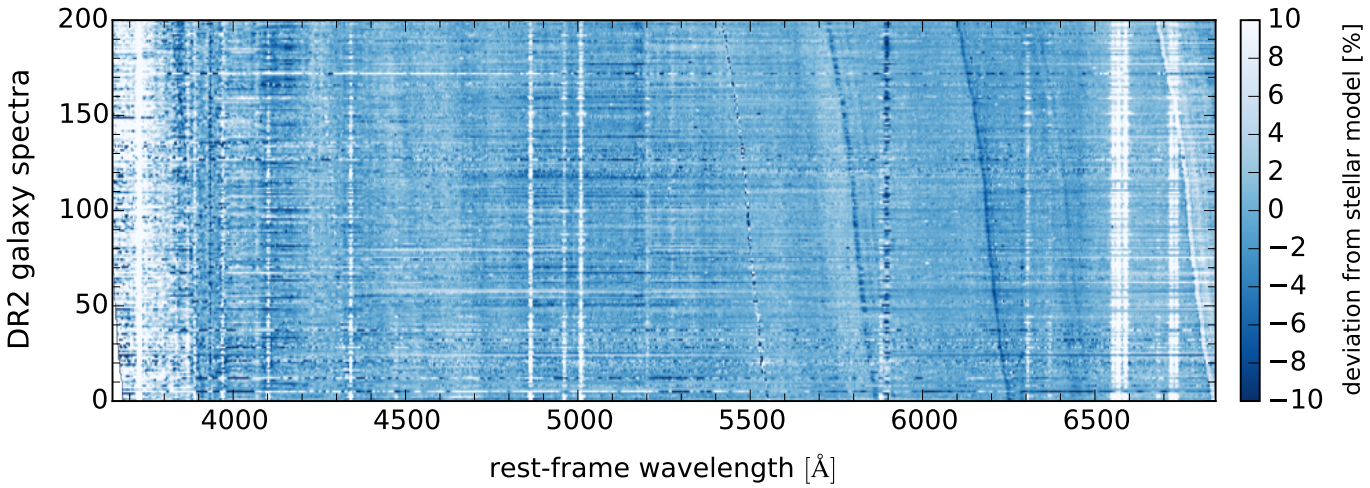

Fig. 18. Relative spectral deviations —$(O_\lambda - M_\lambda)/O_\lambda$, where O and M denote the observed and the model spectra, respectively— for the nuclear regions of all DR2 galaxies, vertically sorted by redshift. Unlike in Fig. 17, emission lines and bad-pixels are not masked in this plot. Systematic deviations from the STARLIGHT model appear as vertical stripes (rest-frame mismatches, e.g. imperfect stellar model or emission lines), while slanted stripes trace observed-frame mismatches (e.g. imperfect sky model). Compare to Fig. 16 of H13.

Alonso-Herrero, A., Rosales-Ortega, F. F., Sánchez, S. F., et al. 2012, MNRAS, 425, L46
Barrera-Ballesteros, J. K., Falcón-Barroso, J., García-Lorenzo, B., et al. 2014, A&A, 568, A70
Bershady, M. A., Verheijen, M. A. W., Swaters, R. A., et al. 2010, ApJ, 716, 198
Blanton, M. R., Schlegel, D. J., Strauss, M. A., et al. 2005, AJ, 129, 2562
Cappellari, M. & Copin, Y. 2003, MNRAS, 342, 345
Cappellari, M., Emsellem, E., Krajnović, D., et al. 2011, MNRAS, 413, 813
Cid Fernandes, R., González Delgado, R. M., García Benito, R., et al. 2014, A&A, 561, A130
Cid Fernandes, R., Mateus, A., Sodré, L., Stasińska, G., & Gomes, J. M. 2005, MNRAS, 358, 363
Cid Fernandes, R., Pérez, E., García Benito, R., et al. 2013, A&A, 557, A86
Croom, S. M., Lawrence, J. S., Bland-Hawthorn, J., et al. 2012, MNRAS, 421, 872
Davies, R. L., Kewley, L. J., Ho, I., & Dopita, M. A. 2014, ArXiv e-prints
De Geyter, G., Baes, M., Camps, P., et al. 2014, MNRAS, 441, 869
Dowler, P., Rixon, G., & Tody, D. 2011, ArXiv e-prints
Erwin, P. 2014, ArXiv e-prints
Fruchter, A. S. & Hook, R. N. 2002, PASP, 114, 144
Galbany, L., Stanishev, V., Mourão, A. M., et al. 2014, ArXiv e-prints
Garcia-Lorenzo, B., Marquez, I., Barrera-Ballesteros, J. K., et al. 2014, ArXiv e-prints
González Delgado, R. M., Cerviño, M., Martins, L. P., Leitherer, C., & Hauschildt, P. H. 2005, MNRAS, 357, 945
González Delgado, R. M., Cid Fernandes, R., García-Benito, R., et al. 2014a, ApJ, 791, L16
González Delgado, R. M., Pérez, E., Cid Fernandes, R., et al. 2014b, A&A, 562, A47
Greisen, E. W. & Calabretta, M. R. 2002, A&A, 395, 1061
Holwerda, B. W. & Keel, W. C. 2013, A&A, 556, A42
Husemann, B., Jahnke, K., Sánchez, S. F., et al. 2013, A&A, 549, A87
Iglesias-Páramo, J., Vílchez, J. M., Galbany, L., et al. 2013, A&A, 553, L7
Kehrig, C., Monreal-Ibero, A., Papaderos, P., et al. 2012, A&A, 540, A11
Kelz, A., Verheijen, M. A. W., Roth, M. M., et al. 2006, PASP, 118, 129
Law, D. R. & MaNGA Team. 2014, in American Astronomical Society Meeting Abstracts, Vol. 223, American Astronomical Society Meeting Abstracts #223, 254.31
Marino, R. A., Rosales-Ortega, F. F., Sánchez, S. F., et al. 2013, A&A, 559, A114
Mármol-Queraltó, E., Sánchez, S. F., Marino, R. A., et al. 2011, A&A, 534, A8
Martínez-García, E. E., Puerari, I., Rosales-Ortega, F. F., et al. 2014, ArXiv e-prints
Mast, D., Rosales-Ortega, F. F., Sánchez, S. F., et al. 2014, A&A, 561, A129
Papaderos, P., Gomes, J. M., Vílchez, J. M., et al. 2013, A&A, 555, L1
Pérez, E., Cid Fernandes, R., González Delgado, R. M., et al. 2013, ApJ, 764, L1
Rosales-Ortega, F. F., Díaz, A. I., Kennicutt, R. C., & Sánchez, S. F. 2011, MNRAS, 415, 2439
Rosales-Ortega, F. F., Kennicutt, R. C., Sánchez, S. F., et al. 2010, MNRAS, 405, 735
Rosales-Ortega, F. F., Sánchez, S. F., Iglesias-Páramo, J., et al. 2012, ApJ, 756, L31
Roth, M. M., Kelz, A., Fechner, T., et al. 2005, PASP, 117, 620
Sánchez, S. F., Cardiel, N., Verheijen, M. A. W., Pedraz, S., & Covone, G. 2007, MNRAS, 376, 125
Sánchez, S. F., Kennicutt, R. C., Gil de Paz, A., et al. 2012a, A&A, 538, A8
Sánchez, S. F., Rosales-Ortega, F. F., Iglesias-Páramo, J., et al. 2014, A&A, 563, A49
Sánchez, S. F., Rosales-Ortega, F. F., Jungwiert, B., et al. 2013, A&A, 554, A58
Sánchez, S. F., Rosales-Ortega, F. F., Kennicutt, R. C., et al. 2011, MNRAS, 410, 313
Sánchez, S. F., Rosales-Ortega, F. F., Marino, R. A., et al. 2012b, A&A, 546, A2
Sanchez-Blazquez, P., Rosales-Ortega, F., Mendez-Abreu, J., et al. 2014, ArXiv e-prints
Sharp, R., Allen, J. T., Fogarty, L. M. R., et al. 2014, ArXiv e-prints
Singh, R., van de Ven, G., Jahnke, K., et al. 2013, A&A, 558, A43
Tody, D., Plante, R., & Harrison, P. 2011, ArXiv e-prints
Vazdekis, A., Sánchez-Blázquez, P., Falcón-Barroso, J., et al. 2010, MNRAS, 404, 1639
Verheijen, M. A. W., Bershady, M. A., Andersen, D. R., et al. 2004, Astronomische Nachrichten, 325, 151
Viironen, K., Sánchez, S. F., Marmol-Queraltó, E., et al. 2012, A&A, 538, A144
Walcher, C. J., Wisotzki, L., Bekeraité, S., et al. 2014, ArXiv e-prints
Wild, V., Rosales-Ortega, F., Falcón-Barroso, J., et al. 2014, A&A, 567, A132

[1] Instituto de Astrofísica de Andalucía (IAA/CSIC), Glorieta de la Astronomía s/n Aptdo. 3004, E-18080 Granada, Spain e-mail: rgb@iaa.es
[2] INAF-Osservatorio Astrofisico di Arcetri - Largo Enrico Fermi, 5 - I-50125 Firenze, Italy
[3] Instituto de Astronomía, Universidad Nacional Autonóma de México, A.P. 70-264, 04510, México, D.F.

Table 1. CALIFA DR2 galaxies and their characteristics.

Name	ID[a]	α(J2000)[b]	δ(J2000)[b]	z[c]	m_g[d]	m_z[d]	$m_u - m_z$[d]	type[e]	bar[f]	b/a[g]
IC5376	001	00:01:19.779	+34:31:32.409	0.0168	14.24	12.60	3.48	Sb	A	0.27
UGC00005	002	00:03:05.643	-01:54:49.804	0.0243	13.88	12.53	2.95	Sbc	A	0.54
NGC7819	003	00:04:24.505	+31:28:19.228	0.0167	14.06	13.01	2.12	Sc	A	0.53
IC1528	005	00:05:05.377	-07:05:36.204	0.0128	13.46	12.52	2.43	Sbc	AB	0.36
UGC00036	007	00:05:13.882	+06:46:19.306	0.0210	14.12	12.46	3.55	Sab	AB	0.60
NGC0001	008	00:07:15.860	+27:42:29.096	0.0151	13.46	12.01	2.97	Sbc	A	0.80
NGC0036	010	00:11:22.298	+06:23:21.667	0.0203	13.46	12.01	3.23	Sb	B	0.65
MCG-02-02-030	013	00:30:07.309	-11:06:49.066	0.0118	13.41	12.08	2.91	Sb	AB	0.34
UGC00312	014	00:31:23.922	+08:28:00.232	0.0145	13.76	13.07	1.52	Sd	B	0.35
UGC00335NED02	017	00:33:57.323	+07:16:05.781	0.0183	14.27	12.82	3.42	E4(x)	A	0.63
NGC0169	022	00:36:51.608	+23:59:27.501	0.0154	14.04	11.74	4.50	Sab(x)	A	0.42
NGC0171	023	00:37:21.552	-19:56:03.210	0.0131	13.21	11.73	3.29	Sb	B	0.63
NGC0180	025	00:37:57.703	+08:38:06.588	0.0177	13.51	11.98	3.00	Sb	B	0.64
NGC0192	026	00:39:13.414	+00:51:50.968	0.0140	13.37	11.72	3.23	Sab	AB	0.31
NGC0216	027	00:41:27.170	-21:02:40.826	0.0052	13.55	12.78	1.78	Sd	A	0.27
NGC0237	030	00:43:27.841	-00:07:29.747	0.0139	13.52	12.38	2.44	Sc	B	0.57
IC1652	037	01:14:56.277	+31:56:54.606	0.0173	14.08	12.72	3.13	S0a	A	0.31
NGC0444	039	01:15:49.562	+31:04:50.245	0.0161	14.47	13.48	2.20	Scd	A	0.24
UGC00809	040	01:15:51.837	+33:48:38.532	0.0140	14.81	13.74	2.52	Scd	A	0.19
UGC00841	041	01:19:10.028	+33:01:50.248	0.0186	14.91	13.73	2.55	Sbc	A	0.25
NGC0477	042	01:21:20.483	+40:29:17.332	0.0196	14.43	13.09	2.66	Sbc	AB	0.66
IC1683	043	01:22:38.929	+34:26:13.654	0.0162	14.11	12.63	2.98	Sb	AB	0.59
NGC0499	044	01:23:11.496	+33:27:36.683	0.0146	12.76	11.19	3.49	E5	A	0.61
NGC0496	045	01:23:11.595	+33:31:45.386	0.0201	13.92	12.93	2.25	Scd	A	0.58
NGC0528	050	01:25:33.571	+33:40:17.198	0.0161	13.51	11.89	3.58	S0	A	0.49
UGC01057	053	01:28:53.253	+13:47:37.674	0.0212	14.54	13.26	2.66	Sc	AB	0.30
NGC0774	072	01:59:34.729	+14:00:29.536	0.0154	13.52	11.88	3.50	S0	A	0.72
NGC0776	073	01:59:54.525	+23:38:39.392	0.0164	13.52	12.06	3.19	Sb	B	0.69
NGC0810	076	02:05:28.562	+13:15:05.867	0.0257	13.70	11.93	3.74	E5(x)	A	0.69
NGC0825	077	02:08:32.329	+06:19:25.200	0.0113	13.63	12.04	3.29	Sa	A	0.33
UGC01938	088	02:28:22.137	+23:12:52.655	0.0213	14.70	13.31	2.90	Sbc	AB	0.25
NGC1056	100	02:42:48.312	+28:34:26.961	0.0052	13.00	11.41	3.02	Sa	A	0.57
UGC02222	103	02:45:09.676	+32:59:22.935	0.0166	13.76	12.29	3.32	S0a(x)	AB	0.51
UGC02229	104	02:45:27.567	+00:54:51.657	0.0244	14.16	12.48	3.49	S0a(x)	A	0.57
UGC02403	115	02:55:57.257	+00:41:33.378	0.0137	14.15	12.41	3.44	Sb	B	0.28
NGC1349	127	03:31:27.512	+04:22:51.241	0.0220	13.34	11.80	3.45	E6	A	0.89
NGC1542	131	04:17:14.172	+04:46:54.239	0.0125	13.60	12.14	3.00	Sab	AB	0.38
UGC03107	133	04:37:21.852	+09:32:40.747	0.0283	14.89	13.35	3.19	Sb	A	0.24
NGC1645	134	04:44:06.400	-05:27:56.414	0.0163	13.46	11.97	3.38	S0a	B	0.64
IC2095	141	04:48:45.881	-05:07:28.668	0.0095	15.59	15.23	1.28	Sc	AB	0.15
UGC03253	146	05:19:41.885	+84:03:09.432	0.0138	13.69	12.27	3.07	Sb	B	0.62
NGC2253	147	06:43:41.836	+65:12:22.950	0.0120	13.26	11.79	2.97	Sbc	B	0.87
UGC03539	148	06:48:54.003	+66:15:41.885	0.0110	14.95	14.13	2.31	Sc	AB	0.19
NGC2347	149	07:16:04.087	+64:42:40.776	0.0149	13.18	11.65	3.08	Sbc	AB	0.64
UGC03899	150	07:32:37.749	+35:36:52.125	0.0130	14.99	14.46	1.47	Sd	A	0.43
NGC2410	151	07:35:02.261	+32:49:19.566	0.0156	13.37	11.78	3.29	Sb	AB	0.32
UGC03969	153	07:41:14.343	+27:36:50.635	0.0275	15.03	13.42	3.21	Sb	A	0.18
UGC03995	155	07:44:09.128	+29:14:50.751	0.0159	13.48	11.92	3.58	Sb	B	0.46
NGC2449	156	07:47:20.299	+26:55:48.708	0.0163	13.70	12.22	3.37	Sab	AB	0.50
UGC04132	165	07:59:13.046	+32:54:52.822	0.0174	13.80	12.23	3.17	Sbc	AB	0.26
UGC04722	231	09:00:24.130	+25:36:53.079	0.0058	15.16	15.07	1.25	Sdm	A	0.19
NGC2730	232	09:02:15.824	+16:50:17.841	0.0128	13.93	13.13	1.95	Scd	B	0.64
NGC2880	272	09:29:34.567	+62:29:26.052	0.0051	12.40	10.99	3.21	E7	AB	0.71
IC2487	273	09:30:09.166	+20:05:27.042	0.0145	13.94	12.58	2.90	Sc	AB	0.22
IC0540	274	09:30:10.338	+07:54:09.903	0.0069	14.24	12.76	3.17	Sab	AB	0.30
NGC2906	275	09:32:06.218	+08:26:30.367	0.0071	12.89	11.46	3.37	Sbc	A	0.51
NGC2916	277	09:34:57.601	+21:42:18.940	0.0124	13.37	11.86	3.16	Sbc	A	0.59
UGC05108	278	09:35:26.279	+29:48:45.439	0.0271	14.35	12.73	3.35	Sb	B	0.77
UGC05358	306	09:58:47.135	+11:23:19.318	0.0097	15.12	14.41	1.79	Sd	B	0.33
UGC05359	307	09:58:51.647	+19:12:53.918	0.0283	14.74	13.43	2.93	Sb	B	0.37

Table 1. continued.

Name	ID[a]	α(J2000)[b]	δ(J2000)[b]	z[c]	m_g[d]	m_z[d]	$m_u - m_z$[d]	type[e]	bar[f]	b/a[g]
UGC05396	309	10:01:40.485	+10:45:23.140	0.0181	14.43	13.24	2.66	Sbc	AB	0.27
NGC3106	311	10:04:05.251	+31:11:07.653	0.0207	13.41	12.01	3.31	Sab	A	0.93
UGC05498NED01	314	10:12:03.658	+23:05:07.590	0.0210	14.65	12.95	3.48	Sa(x)	A	0.24
NGC3160	319	10:13:55.115	+38:50:34.534	0.0229	14.64	12.92	3.63	Sab	AB	0.29
UGC05598	326	10:22:14.004	+20:35:21.879	0.0188	14.80	13.52	2.77	Sb	A	0.30
NGC3303	340	10:37:00.088	+18:08:09.194	0.0200	14.24	12.55	3.56	S0a(x)	AB	0.60
UGC05771	341	10:37:19.340	+43:35:15.321	0.0248	14.10	12.43	3.58	E6	A	0.71
NGC3381	353	10:48:24.818	+34:42:41.078	0.0054	13.41	12.68	1.82	Sd	B	0.71
UGC06036	364	10:55:55.261	+36:51:41.468	0.0218	14.14	12.47	3.65	Sa	A	0.29
IC0674	381	11:11:06.361	+43:37:58.812	0.0251	14.07	12.57	3.40	Sab	B	0.65
NGC3614	388	11:18:21.332	+45:44:53.408	0.0077	13.60	12.37	2.90	Sbc	AB	0.72
NGC3811	436	11:41:16.630	+47:41:26.920	0.0102	13.48	12.06	3.00	Sbc	B	0.62
NGC3991	475	11:57:30.959	+32:20:13.289	0.0108	14.08	13.52	1.42	Sm	A	0.22
NGC3994	476	11:57:36.866	+32:16:39.426	0.0103	13.46	11.98	2.87	Sbc	AB	0.47
NGC4003	479	11:57:59.033	+23:07:29.636	0.0219	13.96	12.39	3.29	S0a	B	0.42
UGC07012	486	12:02:03.146	+29:50:52.737	0.0102	14.41	13.81	1.73	Scd	AB	0.54
NGC4149	502	12:10:32.849	+58:18:14.884	0.0103	13.86	12.30	3.10	Sa	AB	0.19
NGC4185	515	12:13:22.192	+28:30:39.468	0.0130	13.27	12.01	3.03	Sbc	AB	0.64
NGC4210	518	12:15:15.842	+65:59:07.156	0.0091	13.44	12.03	2.99	Sb	B	0.73
IC0776	528	12:19:03.120	+08:51:22.153	0.0081	14.74	14.42	1.25	Sdm	A	0.56
NGC4470	548	12:29:37.778	+07:49:27.129	0.0079	12.96	12.12	1.84	Sc	A	0.66
NGC4644	569	12:42:42.664	+55:08:43.897	0.0165	14.41	13.02	3.00	Sb	A	0.45
NGC4676A	577	12:46:10.107	+30:43:54.899	0.0222	14.78	13.08	2.99	Sdm(x)	AB	0.28
NGC4874	592	12:59:35.709	+27:57:33.339	0.0239	12.89	11.37	3.42	E0	A	0.88
UGC08107	593	12:59:39.778	+53:20:28.203	0.0277	14.30	12.71	3.45	Sa(x)	A	0.39
UGC08231	606	13:08:37.555	+54:04:27.737	0.0083	14.44	13.97	1.45	Sd	AB	0.37
UGC08234	607	13:08:46.505	+62:16:18.099	0.0270	13.45	12.23	2.92	S0	A	0.63
NGC5000	608	13:09:47.487	+28:54:24.993	0.0187	13.94	12.50	2.97	Sbc	B	0.60
UGC08250	609	13:10:20.138	+32:28:59.479	0.0176	15.17	14.03	2.39	Sc	A	0.19
UGC08267	610	13:11:11.334	+43:43:34.787	0.0242	14.87	13.14	3.39	Sb	AB	0.20
NGC5205	630	13:30:03.571	+62:30:41.624	0.0059	13.45	12.12	2.92	Sbc	B	0.67
NGC5216	633	13:32:06.896	+62:42:02.392	0.0098	13.58	12.12	3.27	E0	A	0.91
UGC08733	657	13:48:38.994	+43:24:44.830	0.0078	14.70	13.63	1.83	Sdm	B	0.49
IC0944	663	13:51:30.868	+14:05:31.959	0.0234	13.67	11.95	3.59	Sab	A	0.30
UGC08778	664	13:52:06.669	+38:04:01.273	0.0108	14.20	12.90	2.89	Sb	A	0.21
UGC08781	665	13:52:22.745	+21:32:21.669	0.0253	13.92	12.49	3.31	Sb	B	0.52
NGC5378	676	13:56:51.013	+37:47:50.055	0.0100	13.53	12.12	3.23	Sb	B	0.63
NGC5394	680	13:58:33.201	+37:27:13.118	0.0114	14.39	13.59	2.29	Sbc(x)	B	0.74
NGC5406	684	14:00:20.120	+38:54:55.528	0.0180	13.37	11.84	3.46	Sb	B	0.88
NGC5485	708	14:07:11.349	+55:00:05.933	0.0064	12.41	10.88	3.42	E5	A	0.81
UGC09067	714	14:10:45.458	+15:12:33.858	0.0262	14.29	13.09	2.61	Sbc	AB	0.45
NGC5520	715	14:12:22.811	+50:20:54.309	0.0063	13.31	12.05	2.71	Sbc	A	0.57
NGC5614	740	14:24:07.588	+34:51:31.869	0.0130	12.68	11.03	3.56	Sa(x)	A	0.95
NGC5630	749	14:27:36.610	+41:15:27.919	0.0089	13.60	13.04	1.62	Sdm	B	0.32
NGC5682	758	14:34:44.978	+48:40:12.831	0.0076	14.39	13.64	1.74	Scd	B	0.31
NGC5720	764	14:38:33.281	+50:48:54.874	0.0260	14.13	12.72	3.18	Sbc	B	0.65
UGC09476	769	14:41:32.029	+44:30:45.978	0.0109	13.63	12.61	2.31	Sbc	A	0.63
NGC5784	778	14:54:16.450	+42:33:28.452	0.0181	13.20	11.69	3.45	S0	A	0.81
UGC09665	783	15:01:32.465	+48:19:10.928	0.0085	14.30	12.83	3.12	Sb	A	0.23
NGC5888	789	15:13:07.372	+41:15:52.666	0.0291	13.84	12.25	3.47	Sb	B	0.54
NGC5908	791	15:16:43.191	+55:24:34.461	0.0112	13.12	11.15	3.97	Sa	A	0.24
NGC5930	795	15:26:07.950	+41:40:33.829	0.0088	13.53	11.76	3.27	Sab(x)	AB	0.84
UGC09873	797	15:29:50.651	+42:37:44.104	0.0188	15.19	13.95	2.63	Sb	A	0.21
UGC09892	798	15:32:51.947	+41:11:29.282	0.0189	14.80	13.51	2.78	Sbc	A	0.29
NGC5966	806	15:35:52.108	+39:46:08.047	0.0151	13.24	11.76	3.36	E4	A	0.60
IC4566	807	15:36:42.162	+43:32:21.545	0.0186	13.84	12.35	3.39	Sb	B	0.69
NGC5987	809	15:39:57.356	+58:04:46.249	0.0100	12.76	11.07	3.62	Sa	A	0.39
NGC6004	813	15:50:22.720	+18:56:21.386	0.0128	13.55	12.22	3.02	Sbc	B	0.94
NGC6020	815	15:57:08.137	+22:24:16.492	0.0144	13.40	11.94	3.40	E4	A	0.73
NGC6021	816	15:57:30.685	+15:57:21.766	0.0158	13.63	12.10	3.45	E5	A	0.78
NGC6032	820	16:03:01.124	+20:57:21.330	0.0145	13.97	12.56	2.94	Sbc	B	0.30

Table 1. continued.

Name	ID[a]	α(J2000)[b]	δ(J2000)[b]	z[c]	m_g[d]	m_z[d]	$m_u - m_z$[d]	type[e]	bar[f]	b/a[g]
UGC10205	822	16:06:40.181	+30:05:56.651	0.0219	13.89	12.29	3.32	S0a	A	0.58
NGC6063	823	16:07:12.993	+07:58:44.368	0.0095	13.63	12.53	2.56	Sbc	A	0.60
IC1199	824	16:10:34.347	+10:02:25.322	0.0158	13.97	12.59	2.86	Sb	AB	0.41
NGC6081	826	16:12:56.858	+09:52:01.580	0.0171	13.62	11.93	3.65	S0a	A	0.46
UGC10331	828	16:17:21.123	+59:19:12.466	0.0152	14.50	13.60	2.11	Sc(x)	AB	0.26
NGC6125	829	16:19:11.536	+57:59:02.899	0.0154	12.91	11.39	3.43	E1	A	0.91
NGC6132	831	16:23:38.840	+11:47:10.459	0.0166	14.18	13.09	2.38	Sbc	A	0.36
NGC6146	832	16:25:10.331	+40:53:34.325	0.0292	13.28	11.80	3.40	E5	A	0.77
NGC6154	833	16:25:30.483	+49:50:24.934	0.0199	13.81	12.39	3.33	Sab	B	0.65
UGC10380	834	16:25:49.911	+16:34:33.827	0.0292	14.89	13.18	3.57	Sb	AB	0.28
NGC6150	835	16:25:49.966	+40:29:19.419	0.0292	13.92	12.35	3.49	E7	A	0.48
UGC10384	837	16:26:46.685	+11:34:48.968	0.0165	14.70	13.22	2.82	Sb	A	0.22
UGC10388	838	16:27:02.974	+16:22:56.031	0.0154	14.03	12.67	3.15	Sa	AB	0.40
NGC6173	840	16:29:44.875	+40:48:41.965	0.0294	13.16	11.61	3.49	E6	A	0.65
NGC6168	841	16:31:20.834	+20:11:08.298	0.0086	14.70	13.58	2.30	Sc	AB	0.18
UGC10650	843	17:00:14.583	+23:06:22.839	0.0099	15.35	16.29	0.04	Scd	A	0.20
UGC10693	845	17:04:53.020	+41:51:55.764	0.0280	13.45	12.00	3.41	E7	AB	0.68
UGC10695	846	17:05:05.574	+43:02:35.360	0.0280	13.98	12.42	3.50	E5	A	0.67
UGC10710	847	17:06:52.522	+43:07:19.961	0.0280	14.35	12.75	3.31	Sb	A	0.25
NGC6310	848	17:07:57.480	+60:59:24.569	0.0114	13.72	12.29	3.24	Sb	A	0.22
NGC6314	850	17:12:38.716	+23:16:12.297	0.0221	13.52	12.12	3.09	Sab	A	0.51
NGC6338	851	17:15:22.976	+57:24:40.284	0.0274	13.33	11.70	3.66	E5	A	0.66
UGC10796	852	17:16:47.725	+61:55:12.433	0.0102	14.28	13.74	1.44	Scd	AB	0.49
UGC10811	854	17:18:43.726	+58:08:06.433	0.0291	14.55	13.02	3.30	Sb	B	0.42
IC1256	856	17:23:47.285	+26:29:11.482	0.0159	13.91	12.70	2.60	Sb	AB	0.59
NGC6394	857	17:30:21.423	+59:38:23.613	0.0284	14.53	13.06	3.05	Sbc	B	0.29
UGC10905	858	17:34:06.438	+25:20:38.290	0.0265	13.68	12.15	3.37	S0a	A	0.53
NGC6411	859	17:35:32.849	+60:48:48.255	0.0123	12.73	11.37	3.34	E4	A	0.68
NGC6427	860	17:43:38.599	+25:29:38.178	0.0108	13.28	11.82	3.30	S0	AB	0.61
UGC10972	861	17:46:21.921	+26:32:37.681	0.0155	14.10	12.78	2.91	Sbc	A	0.22
NGC6478	862	17:48:37.742	+51:09:13.683	0.0227	14.16	12.83	2.59	Sc	A	0.42
NGC6497	863	17:51:17.966	+59:28:15.149	0.0105	13.73	12.26	3.41	Sab	B	0.65
NGC6515	864	17:57:25.195	+50:43:41.242	0.0228	13.52	12.10	3.27	E3	A	0.78
UGC11228	865	18:24:46.260	+41:29:33.853	0.0194	13.78	12.26	3.43	S0	B	0.57
UGC11262	866	18:30:35.698	+42:41:33.704	0.0186	14.89	13.75	2.65	Sc	A	0.39
NGC6762	867	19:05:37.090	+63:56:02.791	0.0098	13.81	12.37	3.29	Sab	A	0.49
MCG-02-51-004	868	20:15:39.858	-13:37:19.227	0.0188	13.88	12.47	2.93	Sb	A	0.37
NGC6941	869	20:36:23.474	-04:37:07.459	0.0208	13.47	12.06	3.14	Sb	B	0.73
NGC6978	871	20:52:35.435	-05:42:40.041	0.0199	13.48	11.95	3.27	Sb	AB	0.39
UGC11649	872	20:55:27.620	-01:13:30.879	0.0127	13.47	12.06	3.19	Sab	B	0.88
NGC7025	874	21:07:47.336	+16:20:09.224	0.0166	12.85	11.25	3.57	S0a	A	0.72
UGC11717	877	21:18:35.413	+19:43:07.397	0.0212	14.20	12.45	3.60	Sab	A	0.47
MCG-01-54-016	878	21:25:59.971	-03:48:32.267	0.0098	14.90	14.26	1.56	Scd	A	0.13
UGC11792	880	21:42:12.700	+05:36:55.333	0.0160	14.82	13.30	3.08	Sbc	A	0.20
NGC7194	881	22:03:30.938	+12:38:12.414	0.0272	13.55	12.01	3.47	E3	A	0.79
UGC11958	883	22:14:46.882	+13:50:27.132	0.0262	14.02	12.47	3.44	S0(x)	A	0.74
UGC11982	884	22:18:52.939	-01:03:31.254	0.0162	15.24	14.09	2.68	Scd	A	0.23
UGC12054	885	22:29:32.454	+07:43:33.685	0.0070	14.62	13.82	1.89	Sc	A	0.24
NGC7311	886	22:34:06.797	+05:34:13.166	0.0150	12.60	11.18	3.25	Sa	A	0.49
NGC7321	887	22:36:28.022	+21:37:18.354	0.0238	13.58	12.29	2.98	Sbc	B	0.69
UGC12127	888	22:38:29.421	+35:19:46.894	0.0275	13.46	11.94	3.53	E1	A	0.85
UGC12185	890	22:47:25.063	+31:22:24.672	0.0222	14.16	12.75	3.21	Sb	B	0.47
UGC12224	891	22:52:38.364	+06:05:37.045	0.0118	13.89	12.86	2.60	Sc	A	0.83
NGC7436B	893	22:57:57.546	+26:09:00.012	0.0246	13.40	11.80	3.59	E2(x)	A	0.90
UGC12274	894	22:58:19.600	+26:03:42.974	0.0255	14.21	12.59	3.63	Sa	A	0.36
UGC12308	895	23:01:18.684	+14:20:22.466	0.0076	14.69	14.01	1.82	Scd	A	0.25
NGC7466	896	23:02:03.464	+27:03:09.342	0.0251	14.22	12.76	3.00	Sbc	A	0.53
NGC7489	898	23:07:32.695	+22:59:53.127	0.0208	13.70	12.61	2.42	Sbc	A	0.55
NGC7549	901	23:15:17.271	+19:02:30.437	0.0157	13.98	12.62	2.76	Sbc	B	0.75
NGC7563	902	23:15:55.928	+13:11:46.040	0.0143	13.33	11.80	3.45	Sa	B	0.68
NGC7562	903	23:15:57.495	+06:41:15.151	0.0120	12.10	10.56	3.43	E4	A	0.68

Table 1. continued.

Name	ID[a]	α(J2000)[b]	δ(J2000)[b]	z[c]	m_g[d]	m_z[d]	$m_u - m_z$[d]	type[e]	bar[f]	b/a[g]
NGC7591	904	23:18:16.260	+06:35:08.860	0.0165	13.39	11.80	3.24	Sbc	B	0.59
UGC12519	909	23:20:02.769	+15:57:10.028	0.0146	14.24	12.90	2.87	Sc	AB	0.21
UGC12518	910	23:20:12.737	+07:55:55.915	0.0093	14.74	12.91	3.67	Sb	A	0.23
NGC7625	913	23:20:30.139	+17:13:32.034	0.0054	13.03	11.47	3.03	Sa	A	0.78
NGC7631	914	23:21:26.675	+08:13:03.463	0.0125	13.40	12.05	3.00	Sb	A	0.44
NGC7653	915	23:24:49.358	+15:16:32.165	0.0142	13.17	11.88	3.00	Sb	A	0.88
NGC7671	916	23:27:19.336	+12:28:02.673	0.0135	13.14	11.56	3.56	S0	A	0.65
NGC7683	917	23:29:03.823	+11:26:42.607	0.0124	13.00	11.38	3.61	S0	A	0.62
UGC12688	922	23:35:26.096	+07:19:19.554	0.0174	14.53	13.47	2.29	Scd(x)	AB	0.29
NGC7716	924	23:36:31.450	+00:17:50.179	0.0085	13.03	11.60	3.25	Sb	A	0.71
NGC7738	927	23:44:02.058	+00:30:59.838	0.0228	13.94	12.17	3.56	Sb	B	0.31
UGC12816	930	23:51:50.691	+03:04:57.909	0.0178	14.09	13.16	2.08	Sc	A	0.62
NGC7783NED01	932	23:54:10.078	+00:22:58.299	0.0262	13.62	12.06	3.43	Sa(x)	A	0.46
UGC12864	935	23:57:23.921	+30:59:31.456	0.0156	14.24	13.25	2.19	Sc	B	0.32
MCG-01-01-012	936	23:59:10.803	-04:11:29.763	0.0193	14.64	12.83	4.07	Sab	AB	0.26
NGC7800	937	23:59:36.753	+14:48:25.043	0.0058	13.35	13.16	1.11	Ir	AB	0.40
NGC5947	938	15:30:36.595	+42:43:01.732	0.0198	14.07	12.81	2.80	Sbc	B	0.83
NGC4676B[h]	939	12:46:11.235	+30:43:21.871	0.0218	17.00	15.31	3.44	Sb(x)	B	0.82

Notes. [a] CALIFA unique ID number for the galaxy. [b] Equatorial coordinates of the galaxies as provided by NED. [c] Redshift of the galaxies based on SDSS DR7 spectra or complemented with SIMBAD information if SDSS spectra are not available. [d] Petrosian magnitudes as given by SDSS DR7 database corrected for Galactic extinction. [e] Morphological type from our own visual classification (see W14 for details). "(x)" indicates ongoing mergers. [f] Bar strength of the galaxy as an additional outcome of our visual classification. A stands for non-barred, B for barred and AB if unsure. [g] Ratio between the semi-minor and semi-major axis based on a detailed re-analysis of the SDSS images (see W14 for details). [h] Morphological classification of this particular galaxy NGC 4676B from Wild et al. (2014).

Table 6. CALIFA DR2 quality control parameters for the V500 data

ID	airmass[a]	$\mu_{V,\mathrm{sky}}$[b]	A_V[c]	seeing[d]	flags(O)[e]	δ_λ[f]	S/N(R_{50})[g]	$I_{3\sigma}$[h]	flags(R)[i]	$\left(\frac{g_{\mathrm{CALIFA}}}{g_{\mathrm{SDSS}}}\right)^j$	$\left(\frac{r_{\mathrm{CALIFA}}}{r_{\mathrm{SDSS}}}\right)^k$	flags(C)[l]
001*	1.02 ± 0.01	21.4	0.18	...	000	4.68	24.8	24.0 | 0.9	00000	1.04	1.03	000
002	1.41 ± 0.05	20.9	...	...	00–	4.63	28.9	23.7 | 1.2	00000	0.96	0.98	000
003*	1.01 ± 0.01	20.8	0.23	0.8 ± 0.1	000	5.17	12.8	23.7 | 1.2	00100	0.92	0.97	100
005	1.40 ± 0.01	21.0	...	...	00–	4.65	24.3	23.6 | 1.3	00000	0.99	1.01	000
007*†	1.34 ± 0.05	20.5	...	...	00–	5.21	27.6	23.5 | 1.4	10100	1.03	1.05	000
008	1.34 ± 0.07	21.0	0.20	...	000	4.63	29.1	23.7 | 1.1	00000	1.02	0.99	000
010*	1.31 ± 0.05	21.0	0.22	...	000	4.62	18.2	23.7 | 1.2	00000	1.01	0.98	000
013	1.57 ± 0.10	20.8	0.19	...	000	4.63	31.5	23.6 | 1.3	–00–0	0.96	1.01	001
014*	1.26 ± 0.04	21.0	0.21	...	000	4.62	22.0	23.8 | 1.1	00000	1.03	1.01	000
017	1.23 ± 0.03	21.1	...	...	00–	4.61	9.2	23.6 | 1.3	00000	1.00	1.00	000
022	1.18 ± 0.05	20.9	...	...	00–	4.76	24.8	23.6 | 1.3	10000	0.94	0.94	100
023	1.86 ± 0.03	19.7	0.15	...	110	4.87	14.6	22.8 | 2.7	10011	0.92	0.98	000
025	1.24 ± 0.04	21.0	0.17	...	000	4.63	17.9	23.6 | 1.3	00000	0.98	1.02	001
026	1.26 ± 0.02	20.9	0.13	...	000	4.82	26.3	23.8 | 1.1	00000	0.99	1.00	000
027	1.90 ± 0.01	20.1	0.20	...	110	4.71	30.3	23.5 | 1.5	00010	1.00	1.04	001
030	1.34 ± 0.04	20.9	0.20	...	000	4.65	30.1	23.9 | 1.0	00000	0.99	1.04	101
037	1.58 ± 0.11	20.8	0.17	...	000	4.68	34.7	24.0 | 0.9	00000	1.20	1.25	101
039*	1.03 ± 0.01	20.8	0.23	0.9 ± 0.1	000	5.21	15.6	23.8 | 1.1	01000	0.95	0.99	110
040	1.29 ± 0.06	21.1	0.17	...	000	4.69	24.4	24.0 | 0.9	00000	0.99	1.00	010
041	1.09 ± 0.03	21.1	0.14	...	000	4.95	21.0	23.8 | 1.1	00010	1.02	1.01	000
042*	1.10 ± 0.03	21.0	0.13	...	000	5.21	14.3	23.6 | 1.3	10000	1.08	1.09	101
043*	1.01 ± 0.01	21.3	0.19	...	000	4.79	29.5	23.9 | 1.0	–00–0	1.05	1.02	001
044	1.17 ± 0.04	21.0	...	...	00–	4.79	22.3	23.2 | 1.8	00001	0.96	0.96	000
045	1.28 ± 0.06	20.8	0.14	...	000	5.22	12.6	23.3 | 1.7	10000	0.98	1.03	001
050	1.43 ± 0.08	20.9	0.16	...	000	4.89	37.7	23.7 | 1.2	00000	0.99	1.02	000
053*	1.19 ± 0.04	20.7	...	0.8 ± 0.1	00–	5.25	27.4	23.7 | 1.2	00100	0.95	0.98	000
072	1.16 ± 0.03	21.1	0.15	...	000	4.84	27.3	23.8 | 1.1	00000	1.00	1.02	000
073*	1.04 ± 0.01	21.1	0.20	...	000	4.73	18.6	23.3 | 1.8	00000	1.01	1.01	000
076	1.15 ± 0.03	21.2	0.12	...	000	4.95	16.4	23.4 | 1.6	10000	0.96	0.97	111
077	1.43 ± 0.07	20.9	0.19	...	000	4.64	37.1	23.9 | 1.0	00000	1.05	1.11	101
088*	1.13 ± 0.03	20.8	...	1.0 ± 0.4	00–	5.43	23.7	23.4 | 1.5	01100	0.97	0.99	101
100*	1.37 ± 0.26	20.7	0.14	...	100	5.24	23.5	23.1 | 2.1	10001	0.99	1.00	001
103	1.42 ± 0.08	20.9	0.19	...	000	4.69	28.3	23.6 | 1.3	00000	1.01	1.05	001
104	1.62 ± 0.10	20.8	...	...	00–	4.73	9.4	23.6 | 1.3	00000	1.01	1.00	000
115	1.28 ± 0.02	20.6	...	...	00–	4.67	16.6	23.6 | 1.3	00010	0.98	0.99	000
127*	1.22 ± 0.02	20.6	0.28	0.9 ± 0.1	000	5.12	11.1	23.0 | 2.2	00001	0.93	0.98	000
131	1.20 ± 0.01	21.0	...	...	00–	4.72	22.2	23.3 | 1.8	00000	0.98	0.97	000
133	1.17 ± 0.02	20.6	0.28	0.8 ± 0.1	000	5.13	13.8	23.1 | 2.1	00001	0.88	0.95	100
134	1.47 ± 0.04	21.0	...	...	00–	5.26	20.9	23.2 | 1.9	10101	0.88	0.93	101
141	1.42 ± 0.03	21.0	...	...	00–	4.72	11.3	23.8 | 1.1	00000	1.01	0.97	111
146*†	1.47 ± 0.00	20.7	0.12	...	000	5.79	15.4	23.0 | 2.2	01101	1.03	1.02	001
147	1.15 ± 0.01	21.2	0.14	...	000	5.63	22.7	23.2 | 1.8	01101	0.98	1.00	100
148	1.34 ± 0.04	20.9	0.11	...	000	5.01	17.0	23.6 | 1.2	10000	1.04	0.93	101
149	1.14 ± 0.01	21.4	...	...	00–	5.78	24.8	22.9 | 2.4	11101	0.86	0.91	101
150	1.01 ± 0.01	21.1	...	...	00–	4.76	24.0	23.8 | 1.1	00000	1.00	0.98	010
151*	1.07 ± 0.02	21.0	0.15	...	000	5.85	18.7	23.0 | 2.2	11001	0.88	0.91	101
153	1.19 ± 0.04	21.1	...	...	00–	4.90	25.6	23.7 | 1.2	00000	0.98	0.99	000
155*	1.03 ± 0.01	21.1	0.16	...	000	5.61	14.8	23.1 | 2.0	11001	0.94	0.94	001
156*	1.12 ± 0.04	21.0	0.16	...	000	5.54	19.4	23.3 | 1.7	11000	0.99	1.00	001
165	1.03 ± 0.01	21.1	0.15	...	000	5.98	23.6	23.0 | 2.2	11001	0.92	0.93	100
231	1.03 ± 0.01	21.2	...	...	00–	4.89	8.7	23.9 | 1.0	00000	1.00	0.99	000
232	1.07 ± 0.00	21.1	...	...	00–	4.70	17.1	23.6 | 1.3	00010	1.02	1.01	000
272	1.15 ± 0.01	21.1	...	...	00–	5.19	27.3	23.3 | 1.7	10000	0.97	0.97	000
273*	1.06 ± 0.01	21.1	0.14	...	000	5.33	21.5	23.6 | 1.3	00000	0.98	1.00	001
274*	1.18 ± 0.02	20.9	...	...	00–	4.92	30.1	23.7 | 1.2	00000	1.02	1.03	001
275	1.14 ± 0.00	21.0	...	...	00–	4.93	35.7	23.7 | 1.2	01000	0.99	1.01	000
277*	1.60 ± 0.12	20.3	0.33	...	011	5.65	15.9	22.8 | 2.8	11101	0.95	1.01	101
278	1.32 ± 0.08	20.8	0.12	...	000	5.33	25.8	23.6 | 1.3	00100	1.04	1.05	000
306*	1.28 ± 0.08	20.6	0.17	1.0 ± 0.1	000	4.59	6.5	23.6 | 1.4	00010	1.01	0.96	101
307*	1.06 ± 0.01	21.2	0.16	...	000	5.64	14.3	23.5 | 1.4	01000	0.97	0.97	001

Table 6. continued.

ID	airmass[a]	$\mu_{V,\mathrm{sky}}$[b]	A_V[c]	seeing[d]	flags(O)[e]	δ_λ[f]	S/N(R_{50})[g]	$I_{3\sigma}$[h]	flags(R)[i]	$\left(\frac{g_{\mathrm{CALIFA}}}{g_{\mathrm{SDSS}}}\right)^j$	$\left(\frac{r_{\mathrm{CALIFA}}}{r_{\mathrm{SDSS}}}\right)^k$	flags(C)[l]
309*	1.27 ± 0.05	21.0	0.15	...	000	5.97	12.8	23.1 | 2.1	11001	0.99	0.99	001
311	1.03 ± 0.01	21.3	0.16	...	000	5.96	7.1	23.0 | 2.2	11001	0.87	0.86	101
314	1.13 ± 0.05	21.1	0.15	1.1 ± 0.1	000	4.99	31.1	24.0 | 0.9	00000	1.05	1.07	001
319*	1.11 ± 0.03	20.5	0.56	...	001	5.54	21.7	23.3 | 1.8	01100	0.91	1.00	001
326*	1.05 ± 0.01	20.8	...	...	00–	4.66	24.8	23.9 | 1.0	00000	1.00	1.02	000
340	1.27 ± 0.05	20.9	...	1.1 ± 0.2	00–	5.21	12.7	23.8 | 1.1	01000	0.93	0.95	100
341*	1.17 ± 0.03	...	0.17	1.5 ± 0.2	0–0	5.06	17.0	23.7 | 1.2	00000	1.01	1.03	000
353	1.03 ± 0.02	20.9	...	...	00–	4.74	20.8	23.3 | 1.7	00000	0.98	1.00	001
364*	1.33 ± 0.07	20.8	0.12	...	000	5.39	34.0	23.8 | 1.1	00100	1.01	1.05	000
381	1.01 ± 0.00	21.2	...	...	00–	4.77	32.5	23.9 | 1.0	00000	1.04	1.03	001
388	1.02 ± 0.01	21.1	...	0.2 ± 0.2	00–	5.18	7.8	23.2 | 1.9	00001	0.95	0.94	000
436	1.13 ± 0.03	21.1	0.19	...	000	...	21.7	23.1 | 2.1	0–011	0.97	0.98	000
475*†	1.35 ± 0.07	20.8	0.12	...	000	5.36	21.2	23.7 | 1.2	00000	0.96	1.03	110
476	1.06 ± 0.02	20.8	...	...	00–	4.75	64.0	23.9 | 1.0	00010	1.01	1.03	100
479*	1.14 ± 0.03	20.8	...	...	00–	4.67	28.4	23.9 | 0.9	00010	1.02	1.03	000
486*	1.05 ± 0.03	...	0.16	1.2 ± 0.7	0–0	4.66	22.3	24.0 | 0.9	00000	0.99	0.98	000
502	1.11 ± 0.01	21.3	...	...	00–	5.04	40.3	24.0 | 0.9	00000	1.09	1.07	100
515*	1.01 ± 0.00	20.9	0.14	...	000	5.25	14.9	23.2 | 1.9	00001	0.95	0.98	000
518*	1.16 ± 0.01	20.9	0.15	...	000	5.64	18.6	23.3 | 1.7	01100	0.97	1.00	000
528*	1.14 ± 0.01	20.8	...	...	00–	4.71	7.5	23.7 | 1.2	00000	1.01	1.02	001
548*	1.16 ± 0.01	20.8	0.19	1.2 ± 0.1	000	4.64	43.6	23.8 | 1.1	00010	1.02	1.00	001
569	1.06 ± 0.01	21.2	...	...	00–	4.65	33.8	24.1 | 0.8	10000	0.96	1.01	000
577*†	1.02 ± 0.01	21.0	0.15	...	000	4.95	13.3	24.0 | 0.9	01100	...	...	–0–
592	1.03 ± 0.01	20.9	...	...	00–	4.69	20.0	23.3 | 1.7	00000	0.82	0.84	101
593	1.11 ± 0.02	21.0	...	...	00–	4.73	19.5	23.9 | 1.0	00000	0.98	0.99	000
606	1.07 ± 0.01	21.4	...	...	00–	5.19	15.8	23.9 | 1.0	00000	0.95	1.00	101
607*	1.22 ± 0.03	21.3	0.16	...	000	5.39	41.2	23.6 | 1.3	10000	0.91	0.92	100
608*	1.31 ± 0.06	21.1	...	...	00–	5.87	11.3	23.3 | 1.7	11000	0.91	0.91	101
609*	1.07 ± 0.02	21.3	0.14	...	000	5.55	17.3	23.8 | 1.1	01000	0.99	0.97	100
610*	1.11 ± 0.03	21.2	...	...	00–	5.85	22.7	23.5 | 1.5	11000	0.96	0.97	000
630	1.36 ± 0.04	20.0	...	...	01–	4.64	17.6	23.4 | 1.6	00000	0.99	1.00	001
633	1.13 ± 0.01	21.0	...	...	00–	4.77	13.8	23.7 | 1.2	00000	0.93	0.96	000
657*	1.02 ± 0.01	21.2	0.19	1.1 ± 0.1	000	4.69	10.4	23.9 | 1.0	00000	1.01	1.00	000
663*	1.20 ± 0.04	20.9	...	...	00–	5.32	24.4	23.7 | 1.2	01000	1.01	1.02	100
664*	1.04 ± 0.02	21.2	...	1.1 ± 0.1	00–	5.21	35.6	23.9 | 0.9	00000	1.05	1.06	000
665*	1.06 ± 0.01	21.1	...	...	00–	5.21	18.8	23.7 | 1.2	00000	1.02	1.03	100
676*	1.03 ± 0.03	21.0	0.15	...	000	5.52	12.5	23.2 | 1.8	–10–1	0.96	0.97	100
680*	1.07 ± 0.02	21.0	...	...	00–	4.66	11.8	24.1 | 0.8	00010	1.00	1.03	000
684*	1.05 ± 0.02	21.0	...	...	00–	4.66	25.1	23.5 | 1.5	00000	0.97	0.99	000
708	1.18 ± 0.03	20.8	...	...	00–	4.76	18.8	23.0 | 2.2	00011	0.93	0.95	000
714	1.09 ± 0.01	20.6	0.14	...	000	4.66	28.1	23.8 | 1.0	00010	1.03	1.02	000
715	1.10 ± 0.06	21.1	0.21	...	000	4.74	35.9	24.0 | 0.9	–00–0	1.02	1.04	101
740	1.12 ± 0.03	21.0	...	...	00–	4.66	30.0	23.3 | 1.7	00000	0.96	0.99	001
749	1.08 ± 0.02	21.1	0.19	1.1 ± 0.1	000	4.90	28.9	24.0 | 0.9	00000	1.03	1.04	100
758*	1.02 ± 0.00	21.1	0.24	1.1 ± 0.1	000	4.72	12.2	24.0 | 0.9	00000	0.96	0.97	000
764*	1.29 ± 0.05	21.1	0.18	1.0 ± 0.1	000	4.62	20.0	24.0 | 0.9	00000	1.07	1.02	000
769*	1.02 ± 0.01	21.2	...	...	00–	5.47	18.7	23.6 | 1.3	01100	1.00	1.00	000
778	1.15 ± 0.04	21.2	...	0.9 ± 0.1	00–	4.77	25.3	23.6 | 1.4	00000	0.99	1.00	000
783*	1.08 ± 0.02	21.3	0.16	...	000	5.46	29.3	23.6 | 1.3	00010	0.98	0.98	000
789	1.15 ± 0.03	21.1	0.20	0.9 ± 0.1	000	4.64	27.3	24.0 | 0.9	00010	0.99	0.99	000
791	1.16 ± 0.03	20.9	...	...	00–	4.78	35.6	23.5 | 1.4	00000	0.99	1.01	001
795	1.01 ± 0.00	21.1	...	0.8 ± 0.1	00–	4.71	27.7	23.9 | 1.0	00000	0.97	1.00	000
797*	1.05 ± 0.07	21.0	0.15	...	000	5.11	17.6	24.0 | 0.9	01100	0.99	1.00	000
798*	1.05 ± 0.02	21.3	0.21	...	000	4.66	27.0	24.3 | 0.7	00000	0.97	1.00	000
806*	1.00 ± 0.00	21.1	0.25	1.1 ± 0.1	000	4.70	59.9	23.6 | 1.3	00000	0.85	0.86	101
807	1.16 ± 0.04	20.9	...	...	00–	4.67	18.3	23.4 | 1.5	00010	0.99	1.00	100
809	1.35 ± 0.05	21.0	...	1.0 ± 0.5	00–	4.85	16.2	23.3 | 1.8	00000	0.84	0.87	101
813	1.08 ± 0.01	20.9	0.22	1.4 ± 0.1	000	4.65	19.4	23.6 | 1.4	00010	0.98	0.99	000
815	1.21 ± 0.05	21.1	0.18	0.8 ± 0.1	000	4.82	11.6	23.6 | 1.3	00000	0.96	0.98	000
816	1.21 ± 0.04	20.7	...	0.8 ± 0.1	00–	4.67	34.2	23.8 | 1.1	00010	1.02	1.02	001
820*	1.07 ± 0.02	21.2	0.17	...	000	5.61	7.2	22.9 | 2.5	21001	1.03	1.03	101

Table 6. continued.

ID	airmass[a]	$\mu_{V,\mathrm{sky}}$[b]	A_V[c]	seeing[d]	flags(O)[e]	δ_λ[f]	S/N(R_{50})[g]	$I_{3\sigma}$[h]	flags(R)[i]	$\left(\frac{g_{\mathrm{CALIFA}}}{g_{\mathrm{SDSS}}}\right)^j$	$\left(\frac{r_{\mathrm{CALIFA}}}{r_{\mathrm{SDSS}}}\right)^k$	flags(C)[l]
822*	1.03 ± 0.01	21.2	...	...	00–	6.08	10.1	23.1 | 2.1	11001	0.96	0.96	101
823*	1.15 ± 0.00	20.9	0.19	...	000	4.62	21.3	23.8 | 1.1	10010	0.99	0.98	000
824*†	1.14 ± 0.01	20.9	...	...	00–	4.72	22.9	23.9 | 1.0	00000	0.92	0.89	101
826*	1.18 ± 0.03	21.1	...	...	00–	5.32	26.4	23.7 | 1.2	00100	1.03	1.04	000
828*	1.21 ± 0.03	21.3	0.26	0.9 ± 0.1	000	4.64	27.2	24.0 | 0.9	00000	1.11	1.04	101
829*	1.09 ± 0.01	21.2	0.18	...	000	4.73	17.7	23.4 | 1.6	10000	0.95	0.93	101
831	1.42 ± 0.07	20.2	...	...	01–	4.65	22.3	23.3 | 1.7	00000	1.03	1.02	000
832*	1.01 ± 0.01	21.3	...	...	00–	5.49	23.4	23.5 | 1.5	00100	0.98	0.99	100
833*	1.12 ± 0.03	21.2	0.18	0.9 ± 0.1	000	5.00	18.1	23.8 | 1.1	00100	1.02	0.98	000
834	1.39 ± 0.07	20.5	0.29	...	010	4.70	28.0	23.9 | 1.0	00000	1.17	1.23	101
835*	1.00 ± 0.00	21.1	...	1.1 ± 0.2	00–	5.28	38.2	24.0 | 0.9	01000	0.98	1.01	000
837*	1.11 ± 0.00	21.1	0.17	0.9 ± 0.1	000	4.84	43.0	24.1 | 0.8	01000	1.07	1.03	001
838	1.46 ± 0.09	20.3	...	...	01–	4.65	25.7	23.6 | 1.4	00000	1.06	1.06	000
840*	1.18 ± 0.04	21.0	0.28	0.9 ± 0.1	000	4.65	3.0	23.5 | 1.4	00000	1.02	0.96	100
841	1.16 ± 0.04	21.2	...	0.9 ± 0.1	00–	4.71	24.0	23.6 | 1.3	00000	1.01	1.03	001
843*	1.45 ± 0.09	21.0	0.23	0.8 ± 0.1	000	4.60	9.3	23.8 | 1.1	00000	1.08	1.05	011
845*	1.03 ± 0.02	21.4	0.19	...	000	4.64	16.0	23.8 | 1.1	00000	0.93	0.95	100
846*	1.06 ± 0.02	21.0	0.39	0.8 ± 0.1	001	4.64	7.7	23.7 | 1.2	00000	0.97	0.98	000
847*	1.31 ± 0.09	21.3	0.15	0.7 ± 0.1	010	4.66	20.4	24.0 | 0.9	20000	1.16	1.25	101
848*	1.10 ± 0.00	21.0	0.38	0.9 ± 0.1	001	4.74	32.3	23.8 | 1.1	00000	1.02	1.01	000
850*	1.05 ± 0.01	21.0	0.29	...	000	4.66	29.6	23.7 | 1.2	00000	1.00	1.01	000
851*	1.32 ± 0.04	20.5	0.41	0.7 ± 0.1	001	4.66	9.5	23.3 | 1.7	00010	0.93	0.93	100
852*	1.12 ± 0.01	21.0	0.36	0.9 ± 0.1	001	4.76	8.1	23.8 | 1.1	00000	1.01	0.99	000
854*	1.18 ± 0.03	20.7	0.42	0.9 ± 0.1	001	4.68	20.3	23.6 | 1.3	00010	1.00	1.01	001
856*	1.05 ± 0.02	21.2	0.17	...	000	4.61	24.1	23.9 | 1.0	00000	0.99	0.99	000
857*	1.08 ± 0.00	21.5	0.16	0.9 ± 0.1	000	4.67	36.7	24.2 | 0.8	00000	0.98	1.01	000
858*	1.10 ± 0.03	21.2	0.15	1.3 ± 0.2	000	4.67	15.8	23.7 | 1.2	00000	1.01	0.98	000
859*	1.16 ± 0.02	21.2	0.15	0.7 ± 0.1	000	4.67	11.0	23.6 | 1.4	00000	0.92	0.95	000
860*	1.04 ± 0.02	21.2	0.29	1.0 ± 0.1	000	4.60	41.5	23.6 | 1.3	00000	1.10	1.06	101
861	1.08 ± 0.02	21.1	...	...	00–	4.62	22.4	23.5 | 1.4	00000	1.04	1.06	001
862	1.13 ± 0.03	20.8	...	1.1 ± 0.2	00–	5.19	20.3	23.4 | 1.6	00100	0.99	1.01	001
863*	1.09 ± 0.01	21.4	0.16	0.7 ± 0.1	000	4.67	29.4	24.1 | 0.8	00000	1.02	1.05	001
864*	1.06 ± 0.01	20.9	0.28	...	000	4.70	12.2	23.5 | 1.5	20010	0.99	0.98	100
865*	1.01 ± 0.01	21.2	0.25	...	000	4.71	32.4	23.9 | 1.0	10000	1.01	1.02	001
866*	1.04 ± 0.02	21.3	0.21	1.1 ± 0.1	000	4.64	12.6	24.0 | 0.9	20000	1.04	1.02	000
867*	1.13 ± 0.01	21.2	0.21	1.1 ± 0.1	000	4.69	39.2	24.0 | 0.9	10000	1.08	1.09	001
868	1.65 ± 0.04	20.1	...	...	01–	4.84	25.3	23.3 | 1.7	–00–0	0.96	0.99	001
869	1.41 ± 0.06	20.8	0.19	1.1 ± 0.1	000	4.66	16.4	23.5 | 1.5	00000	1.04	1.02	101
871	1.38 ± 0.01	20.6	0.17	0.9 ± 0.1	000	4.70	21.3	23.4 | 1.6	–00–0	0.99	1.02	100
872*	1.28 ± 0.01	20.9	0.15	0.6 ± 0.1	000	4.66	18.2	23.4 | 1.5	00010	0.98	0.98	000
874*	1.10 ± 0.02	21.0	0.22	...	000	4.75	24.4	23.2 | 1.9	00001	1.01	1.03	101
877*†	1.24 ± 0.05	21.0	0.22	...	000	4.72	16.8	23.6 | 1.3	20000	1.23	1.23	101
878*	1.33 ± 0.01	20.9	0.22	0.9 ± 0.1	000	4.59	6.8	23.7 | 1.1	00010	1.01	0.99	101
880	1.24 ± 0.03	20.7	0.29	0.9 ± 0.1	000	4.63	24.2	23.6 | 1.3	00010	0.93	0.94	100
881*	1.10 ± 0.00	21.1	0.15	0.8 ± 0.1	000	4.67	18.2	23.8 | 1.1	00010	0.94	0.94	000
883*	1.10 ± 0.01	21.2	0.17	1.0 ± 0.2	000	4.63	10.1	23.6 | 1.3	00000	0.99	0.95	101
884	1.66 ± 0.10	20.4	...	...	01–	4.90	10.8	23.4 | 1.5	00000	0.97	0.98	110
885	1.25 ± 0.04	20.9	0.20	0.7 ± 0.1	000	4.88	25.4	23.7 | 1.2	00100	1.04	1.01	001
886	1.29 ± 0.04	21.0	0.17	0.9 ± 0.2	000	4.65	40.5	23.4 | 1.5	00000	1.01	1.00	000
887*	1.08 ± 0.02	21.3	0.17	0.9 ± 0.1	000	4.67	31.9	23.9 | 1.0	00000	1.01	0.98	001
888*	1.01 ± 0.01	20.9	0.22	...	000	4.68	2.5	23.5 | 1.5	00010	0.93	0.94	000
890*	1.08 ± 0.02	21.0	0.22	...	000	4.71	29.9	23.9 | 1.0	00010	1.00	1.01	000
891	1.37 ± 0.06	20.3	0.21	1.2 ± 0.2	010	5.23	9.2	23.1 | 2.0	00101	0.91	0.98	000
893*	1.35 ± 0.07	20.5	0.20	1.0 ± 0.1	000	5.32	6.9	22.9 | 2.6	20111	0.89	0.92	111
894	1.31 ± 0.06	20.5	...	0.9 ± 0.1	00–	4.74	21.3	23.6 | 1.3	00010	1.06	1.11	101
895	1.15 ± 0.03	20.5	0.22	1.1 ± 0.1	000	5.15	10.3	23.5 | 1.4	00000	0.94	0.97	100
896*	1.36 ± 0.08	20.8	0.18	0.9 ± 0.1	000	5.01	21.8	23.8 | 1.1	00100	1.04	1.02	001
898	1.60 ± 0.11	20.4	...	0.9 ± 0.1	01–	4.66	12.4	22.9 | 2.5	00011	0.97	1.00	000
901*	1.10 ± 0.03	21.3	0.14	1.0 ± 0.1	000	4.63	29.9	23.7 | 1.2	20000	0.97	1.03	101
902*	1.10 ± 0.00	21.2	0.17	0.8 ± 0.1	000	4.71	39.3	23.6 | 1.3	00000	1.06	1.01	001
903	1.45 ± 0.08	20.9	...	...	00–	4.64	30.5	23.3 | 1.8	00000	0.97	0.97	001

Table 6. continued.

ID	airmass[a]	$\mu_{V,\mathrm{sky}}$[b]	A_V[c]	seeing[d]	flags(O)[e]	δ_λ[f]	S/N(R_{50})[g]	$I_{3\sigma}$[h]	flags(R)[i]	$\left(\frac{g_{\mathrm{CALIFA}}}{g_{\mathrm{SDSS}}}\right)$[j]	$\left(\frac{r_{\mathrm{CALIFA}}}{r_{\mathrm{SDSS}}}\right)$[k]	flags(C)[l]
904*	1.20 ± 0.04	21.0	0.17	0.9 ± 0.1	000	4.71	21.5	23.6 | 1.4	00000	1.01	0.98	000
909	1.09 ± 0.02	20.8	...	...	00–	5.05	29.5	23.8 | 1.1	00000	1.02	1.00	000
910	1.22 ± 0.03	21.1	...	...	00–	4.62	18.7	23.4 | 1.6	00000	0.99	1.01	101
913	1.47 ± 0.09	21.1	...	...	00–	4.63	38.8	23.4 | 1.6	00000	0.96	1.01	100
914	1.18 ± 0.02	21.0	0.13	...	000	4.79	31.4	23.8 | 1.1	00000	0.98	1.00	000
915	1.28 ± 0.05	21.1	...	...	00–	4.61	25.4	23.4 | 1.6	00000	1.06	1.03	000
916	1.55 ± 0.10	20.8	...	...	00–	4.65	25.0	23.0 | 2.2	00001	0.95	0.99	101
917	1.21 ± 0.03	20.9	...	...	00–	4.69	31.5	23.5 | 1.4	00010	1.03	1.00	100
922	1.15 ± 0.00	20.8	0.14	...	000	5.20	16.8	23.5 | 1.5	00100	1.06	1.08	101
924	1.43 ± 0.12	20.6	...	...	00–	4.79	12.8	23.0 | 2.3	–00–1	1.01	1.00	000
927	1.29 ± 0.03	21.0	...	...	00–	4.64	14.7	23.8 | 1.1	00000	1.01	1.02	000
930	1.29 ± 0.03	20.8	...	...	00–	4.62	7.3	23.1 | 2.1	00011	1.03	1.04	010
932	1.27 ± 0.02	21.0	...	...	00–	4.71	33.5	23.7 | 1.2	00000	1.00	1.00	100
935*	1.04 ± 0.02	21.0	...	1.1 ± 0.1	00–	5.09	11.1	23.7 | 1.2	00000	0.96	1.00	000
936	1.42 ± 0.05	20.8	0.15	...	000	4.84	30.7	24.0 | 0.9	00000	1.06	1.11	101
937	1.13 ± 0.02	21.0	...	...	00–	4.62	13.8	23.7 | 1.2	00010	0.99	0.97	000
938	1.01 ± 0.01	...	0.16	...	0–0	4.74	31.5	24.0 | 0.9	00000	0.98	1.00	100
939*	1.11 ± 0.04	20.8	0.15	...	000	4.99	8.7	23.6 | 1.3	01110	1.05	1.03	100

Notes. We describe the meaning of each column including the identifier of each column in the electronic table available on the DR2 web page. [a] Mean airmass (OBS_AIR_MEAN) and rms (OBS_AIR_RMS) of the observations for the frames used to create the considered datacube. [b] Average night-sky surface brightness (OBS_SKY_MAG) in the V band during the observations in units of mag arcsec^{-2}. [c] Average night-sky attenuation (OBS_EXT_MEAN) in the V band during the observations in magnitudes. [d] Average natural seeing (OBS_SEEING_MEAN) in the V-band during the observations in arcsec (FWHM). [e] Observation quality flags, combining the three individual column flags (FLAG_OBS_AM, FLAG_OBS_SKYMAG, FLAG_OBS_EXT) as described in Sect. 5. [f] Average spectral resolution (RED_DISP_MEAN) in Å (FWHM), measured by fitting the night-sky emission lines with single Gaussian functions. [g] Average signal-to-noise ratio (CAL_SNR1HLR) estimated for the full wavelength range at one half light radius from the center. [h] Average flux at the 3σ continuum detection limit in units of V-band mag arcsec^{-2} and in units of 10^{-18} erg s^{-1} cm^{-2}Å^{-1} arcsec^{-2}. [i] Reduction/instrumental performance quality flags, combining the five individual column flags (FLAG_RED_STRAYLIGHT, FLAG_RED_DISP, FLAG_RED_CDISP, FLAG_RED_SKYLINES, FLAG_RED_LIMSB) as described in Sect. 5. [j] Ratio between the SDSS g band flux derived from the datacube and the one derived from the SDSS images for a 30″-diameter aperture (CAL_QFLUX_G). [k] Ratio between the SDSS r band flux derived from the datacube and the one derived from the SDSS images for a 30″-diameter aperture (CAL_QFLUX_R). [l] Quality control flags, combining the three individual column flags (FLAG_CAL_SPECPHOTO, FLAG_CAL_WL, FLAG_CAL_IMA) as described in Sect. 5.

Table 7. CALIFA DR2 quality control parameters for the V1200 data

ID	airmass[a]	$\mu_{V,\mathrm{sky}}$[b]	A_V[c]	seeing[d]	flags(O)[e]	δ_λ[f]	S/N(R_{50})[g]	$I_{3\sigma}$[h]	flags(R)[i]	flags(C)[j]
001*	1.01 ± 0.02	...	0.26	...	0–0	1.90	9.0	23.2 | 3.3	00000	000
002	1.32 ± 0.04	21.8	0.13	...	000	1.94	12.4	23.3 | 3.0	00000	000
003*	1.08 ± 0.06	22.0	0.17	...	000	1.96	6.5	23.3 | 2.9	11000	000
005	1.44 ± 0.05	21.8	0.16	...	000	1.94	13.2	23.4 | 2.8	–00–0	100
007*†	1.18 ± 0.02	21.7	0.14	...	000	1.96	10.2	22.8 | 4.9	00000	001
008	1.04 ± 0.03	21.9	0.43	...	001	1.90	10.2	23.2 | 3.3	00010	000
010*	1.29 ± 0.09	22.2	...	...	00–	1.92	6.1	23.0 | 4.1	00000	001
013	1.53 ± 0.04	21.8	0.14	...	000	1.94	16.0	23.4 | 2.9	00010	100
014*	1.27 ± 0.08	22.2	0.19	...	000	1.90	11.4	23.3 | 3.0	00000	000
017	1.19 ± 0.03	21.9	...	...	00–	1.94	4.4	23.5 | 2.5	00000	001
022	1.12 ± 0.08	22.4	0.15	...	000	1.99	6.2	22.7 | 5.3	–00–0	001
023	1.89 ± 0.07	...	...	...	1—-	1.96	8.7	22.9 | 4.3	10010	000
025	1.22 ± 0.06	22.0	0.15	...	000	1.94	8.5	23.1 | 3.5	00010	101
026	1.27 ± 0.03	21.8	...	...	00–	1.91	10.5	23.4 | 2.7	00010	000
027	1.93 ± 0.05	21.3	0.13	...	110	1.95	14.0	23.2 | 3.2	10000	101
030	1.28 ± 0.03	21.9	0.14	...	000	1.94	17.2	23.7 | 2.1	00000	001
037	1.02 ± 0.01	22.2	...	...	00–	1.93	15.7	23.7 | 2.0	00010	001
039*	1.07 ± 0.04	22.1	0.21	1.1 ± 0.2	000	1.96	9.3	23.6 | 2.3	01000	000
040	1.03 ± 0.03	22.2	0.21	...	000	1.93	11.0	23.5 | 2.5	00000	000
041	1.02 ± 0.02	22.3	...	...	00–	1.90	9.9	23.5 | 2.6	00000	000
042*	1.19 ± 0.09	22.3	0.15	0.9 ± 0.1	000	2.01	9.1	23.6 | 2.3	01000	101
043*	1.01 ± 0.01	22.3	0.27	...	000	1.90	11.1	23.4 | 2.7	00000	000
044	1.05 ± 0.04	22.4	0.11	...	000	1.97	7.4	22.7 | 5.3	00110	000
045	1.01 ± 0.01	22.4	0.14	1.2 ± 0.2	000	1.99	9.2	23.5 | 2.4	00000	001
050	1.14 ± 0.07	22.3	0.14	...	000	2.06	16.2	23.2 | 3.3	01000	101
053*	1.33 ± 0.17	21.9	0.16	...	100	2.13	10.3	23.1 | 3.5	01110	000
072	1.13 ± 0.04	21.9	0.12	...	000	1.94	11.4	23.4 | 2.8	00000	000
073*	1.08 ± 0.04	22.2	0.26	...	000	1.91	7.2	22.9 | 4.3	00000	001
076	1.23 ± 0.08	22.2	0.11	...	000	2.09	4.6	22.6 | 5.6	01100	001
077	1.17 ± 0.01	21.8	...	...	00–	1.94	17.3	23.6 | 2.3	00010	001
088*	1.31 ± 0.13	21.4	0.21	...	010	1.99	9.1	22.7 | 5.1	01100	011
100*	1.36 ± 0.14	21.8	0.15	1.1 ± 0.1	000	2.00	13.2	23.1 | 3.7	01000	001
103	1.09 ± 0.09	22.2	...	...	00–	2.01	11.3	22.8 | 4.8	01100	001
104	1.26 ± 0.03	21.9	0.14	...	000	1.94	5.0	23.5 | 2.6	00000	001
115	1.34 ± 0.09	22.1	0.15	...	000	2.01	5.3	22.7 | 5.2	01100	101
127*	1.37 ± 0.27	21.7	0.15	...	100	1.99	4.2	22.5 | 6.4	–00–1	000
131	1.19 ± 0.00	22.3	0.14	...	000	1.99	7.0	22.3 | 7.7	–00–1	000
133	1.13 ± 0.01	21.9	0.16	...	000	2.00	5.5	22.5 | 6.4	–10–1	101
134	1.37 ± 0.01	22.0	...	...	00–	2.00	10.0	23.1 | 3.5	01000	000
141	1.37 ± 0.02	22.0	0.15	...	000	1.98	5.1	23.0 | 4.1	00100	001
146*†	1.48 ± 0.01	22.2	0.14	1.3 ± 0.2	000	2.00	10.7	23.3 | 2.9	01000	001
147	1.16 ± 0.02	22.3	0.14	1.1 ± 0.1	000	1.95	16.3	23.6 | 2.3	00010	001
148	1.29 ± 0.06	22.1	0.12	...	000	1.93	8.2	23.4 | 2.7	00000	001
149	1.27 ± 0.06	22.2	0.11	...	000	1.92	13.2	23.0 | 4.1	10000	001
150	1.06 ± 0.04	22.2	0.15	...	000	1.93	12.4	23.3 | 3.0	10000	000
151*	1.52 ± 0.19	21.4	...	...	11–	2.04	9.7	22.9 | 4.4	01100	001
153	1.09 ± 0.03	21.6	...	...	00–	1.97	10.7	23.1 | 3.4	–00–0	001
155*	1.09 ± 0.05	22.1	0.13	0.9 ± 0.1	000	2.33	4.8	22.5 | 6.2	21110	001
156*	1.08 ± 0.05	22.3	0.14	...	000	2.36	8.1	22.6 | 5.6	01100	001
165	1.25 ± 0.11	21.7	...	...	00–	1.94	15.7	23.1 | 3.5	00100	000
231	1.06 ± 0.03	22.3	...	...	00–	1.92	5.4	23.5 | 2.5	10000	001
232	1.31 ± 0.12	21.9	0.11	...	000	1.96	9.8	23.5 | 2.4	00010	101
272	1.13 ± 0.03	22.1	...	...	00–	2.09	9.2	22.8 | 5.0	01010	000
273*	1.06 ± 0.01	22.2	0.14	1.1 ± 0.1	000	2.01	12.6	23.6 | 2.3	01000	000
274*	1.30 ± 0.09	22.0	...	...	00–	2.05	10.7	23.0 | 4.0	01100	000
275	1.16 ± 0.02	22.4	0.15	...	000	1.99	9.2	22.4 | 6.7	–00–1	000
277*	1.08 ± 0.04	21.7	0.15	...	000	2.13	12.0	23.0 | 4.0	01010	001
278	1.09 ± 0.05	22.5	0.11	...	000	2.24	7.4	22.8 | 4.8	01100	100
306*	1.14 ± 0.03	21.3	...	...	01–	2.02	3.5	23.2 | 3.4	21100	001
307*	1.20 ± 0.08	22.2	0.15	0.8 ± 0.1	000	2.33	4.8	22.7 | 5.2	11100	001

Table 7. continued.

ID	airmass[a]	$\mu_{V,\mathrm{sky}}$[b]	A_V[c]	seeing[d]	flags(O)[e]	δ_λ[f]	S/N(R_{50})[g]	$I_{3\sigma}$[h]	flags(R)[i]	flags(C)[j]
309*	1.25 ± 0.08	22.1	0.14	...	000	2.38	6.3	22.8 | 4.8	01100	000
311	1.03 ± 0.03	22.4	...	...	00–	2.02	4.2	22.9 | 4.3	01100	000
314	1.05 ± 0.01	22.4	0.12	...	000	1.92	11.5	23.2 | 3.3	–00–0	001
319*	1.07 ± 0.06	22.2	0.15	1.1 ± 0.1	000	1.99	12.5	23.6 | 2.3	–01–0	000
326*	1.29 ± 0.05	21.9	...	...	00–	2.02	5.4	22.7 | 5.0	01100	001
340	1.08 ± 0.02	22.5	...	...	00–	2.01	4.0	23.0 | 3.9	01100	001
341*	1.21 ± 0.08	22.0	0.16	1.2 ± 0.1	000	1.91	7.9	23.4 | 2.7	00100	001
353	1.04 ± 0.03	22.5	0.10	...	000	2.07	9.4	23.3 | 2.9	01010	001
364*	1.02 ± 0.02	22.1	...	0.9 ± 0.1	00–	2.03	15.8	23.3 | 2.9	11000	001
381	1.01 ± 0.01	22.2	...	...	00–	1.96	12.4	23.6 | 2.4	–00–0	000
388	1.33 ± 0.11	22.1	...	...	00–	2.15	2.3	22.4 | 6.7	01111	101
436	1.10 ± 0.03	21.4	...	...	01–	1.96	11.1	23.0 | 3.9	–00–0	001
475*†	1.13 ± 0.07	22.1	...	...	00–	2.03	11.6	23.3 | 2.9	21010	101
476	1.40 ± 0.28	21.8	...	...	10–	2.02	25.5	22.9 | 4.5	01100	001
479*	1.16 ± 0.03	22.3	...	...	00–	2.05	7.2	22.7 | 5.3	01100	001
486*	1.21 ± 0.10	22.1	0.15	0.8 ± 0.1	000	1.99	8.6	23.5 | 2.5	10100	100
502	1.23 ± 0.08	21.9	...	...	00–	1.93	11.6	22.5 | 6.1	00000	001
515*	1.20 ± 0.09	22.3	0.15	0.9 ± 0.1	000	2.30	4.2	22.6 | 5.5	11110	000
518*	1.18 ± 0.03	22.6	0.13	...	000	2.03	12.6	23.3 | 2.9	01100	000
528*	1.48 ± 0.08	22.0	...	...	00–	2.10	2.0	22.7 | 5.5	01100	110
548*	1.21 ± 0.05	21.9	0.18	0.8 ± 0.1	000	2.00	14.6	23.2 | 3.3	10000	100
569	1.16 ± 0.05	22.0	0.15	...	000	1.95	15.0	23.5 | 2.4	00000	001
577*†	1.06 ± 0.04	22.2	0.22	...	000	1.89	6.5	23.6 | 2.3	00100	00–
592	1.03 ± 0.02	22.3	...	...	00–	2.25	4.9	22.6 | 5.5	01100	000
593	1.15 ± 0.05	21.9	...	...	00–	1.95	8.3	23.5 | 2.6	00000	010
606	1.33 ± 0.09	22.1	0.17	...	000	1.94	10.4	23.6 | 2.3	00000	001
607*	1.25 ± 0.07	22.3	0.14	...	000	2.25	16.7	23.1 | 3.7	01000	000
608*	1.20 ± 0.10	21.9	0.16	...	000	1.92	6.3	23.2 | 3.3	00000	000
609*	1.08 ± 0.05	22.4	0.15	0.8 ± 0.1	000	2.28	6.8	23.0 | 3.9	11100	011
610*	1.17 ± 0.07	22.5	...	...	00–	2.14	8.9	23.0 | 4.1	11100	100
630	1.26 ± 0.06	22.4	...	...	00–	1.92	10.7	23.3 | 2.9	00000	000
633	1.55 ± 0.12	22.0	...	...	00–	1.92	4.3	23.2 | 3.3	00010	000
657*	1.09 ± 0.05	22.4	0.19	1.5 ± 0.2	000	1.90	5.3	23.7 | 2.1	00000	000
663*	1.10 ± 0.02	22.0	...	...	00–	1.98	11.8	23.3 | 2.9	01000	001
664*	1.07 ± 0.04	22.0	0.26	1.2 ± 0.1	000	1.96	16.2	23.4 | 2.7	00000	001
665*	1.17 ± 0.10	22.1	0.10	...	000	1.95	5.1	22.8 | 4.6	00000	001
676*	1.01 ± 0.02	22.5	0.17	0.8 ± 0.1	000	2.26	4.6	22.9 | 4.2	01100	001
680*	1.07 ± 0.05	22.4	0.10	...	000	1.95	5.4	23.7 | 2.0	00000	000
684*	1.06 ± 0.04	22.3	0.13	0.9 ± 0.1	000	1.96	13.0	23.4 | 2.8	00000	001
708	1.12 ± 0.04	22.2	...	...	00–	1.91	7.7	23.0 | 4.0	00010	000
714	1.43 ± 0.12	21.9	...	...	00–	1.93	12.6	23.4 | 2.7	–00–0	001
715	1.18 ± 0.06	21.9	0.22	...	000	2.00	18.7	23.6 | 2.3	00000	001
740	1.05 ± 0.04	22.8	...	...	00–	2.24	4.4	22.2 | 8.3	01011	001
749	1.07 ± 0.04	22.3	...	...	00–	2.06	13.2	23.4 | 2.7	11010	001
758*	1.18 ± 0.05	22.2	0.26	1.0 ± 0.1	001	1.89	5.5	23.4 | 2.7	–00–0	100
764*	1.11 ± 0.04	...	0.16	...	0–0	2.02	7.7	23.6 | 2.4	01100	001
769*	1.03 ± 0.02	22.2	...	...	00–	2.00	9.6	23.3 | 3.1	01000	000
778	1.02 ± 0.01	22.5	...	...	00–	2.13	8.8	23.2 | 3.3	01000	000
783*	1.20 ± 0.07	22.3	0.17	...	000	2.29	11.3	22.9 | 4.2	01000	000
789	1.10 ± 0.05	22.1	...	...	00–	1.95	12.4	23.5 | 2.6	00000	000
791	1.08 ± 0.02	22.6	...	...	00–	2.28	9.0	22.7 | 5.1	01110	001
795	1.23 ± 0.09	22.3	...	...	00–	1.92	12.3	23.5 | 2.6	00000	000
797*	1.06 ± 0.04	22.5	0.17	1.3 ± 0.2	000	1.89	8.4	23.6 | 2.4	00000	000
798*	1.13 ± 0.07	22.2	0.30	0.8 ± 0.1	001	1.93	8.1	23.4 | 2.8	00000	001
806*	1.06 ± 0.05	22.2	0.21	1.1 ± 0.1	000	1.90	29.0	23.5 | 2.4	00010	000
807	1.30 ± 0.19	22.0	...	...	10–	1.96	9.8	23.5 | 2.5	–00–0	001
809	1.30 ± 0.08	21.7	...	...	00–	1.95	8.2	23.2 | 3.2	00010	001
813	1.07 ± 0.02	22.3	...	...	00–	2.05	8.7	23.1 | 3.7	01010	000
815	1.15 ± 0.10	22.2	...	...	00–	2.05	3.8	23.1 | 3.7	–10–0	001
816	1.15 ± 0.06	22.2	...	...	00–	2.08	12.1	23.3 | 3.0	11010	001
820*	1.15 ± 0.10	22.3	0.15	0.7 ± 0.1	000	2.35	4.3	22.7 | 5.4	–11–0	101

Table 7. continued.

ID	airmass[a]	$\mu_{V,\mathrm{sky}}$[b]	A_V[c]	seeing[d]	flags(O)[e]	δ_t[f]	S/N(R_{50})[g]	$I_{3\sigma}$[h]	flags(R)[i]	flags(C)[j]
822*	1.09 ± 0.05	22.1	0.16	0.8 ± 0.1	000	1.91	7.4	23.4 | 2.9	00000	000
823*	1.17 ± 0.03	22.0	0.26	0.9 ± 0.1	000	1.91	10.3	23.3 | 3.1	00000	001
824*†	1.18 ± 0.04	21.6	0.24	1.1 ± 0.2	000	1.98	6.4	22.6 | 5.7	00000	001
826*	1.16 ± 0.04	22.0	...	...	00–	2.10	10.9	22.9 | 4.5	–11–0	001
828*	1.17 ± 0.04	22.6	0.16	1.0 ± 0.1	000	1.89	12.4	23.6 | 2.2	10000	000
829*	1.24 ± 0.07	22.0	0.17	1.4 ± 0.2	000	1.95	7.1	23.3 | 2.9	01110	000
831	1.18 ± 0.05	21.3	0.17	...	010	1.95	12.5	23.1 | 3.6	10000	000
832*	1.02 ± 0.02	22.1	...	...	00–	2.00	10.4	23.4 | 2.9	–10–0	001
833*	1.07 ± 0.03	22.2	0.10	...	000	1.95	4.6	22.9 | 4.4	00000	001
834	1.27 ± 0.10	22.3	0.23	...	000	2.04	10.5	23.5 | 2.5	01010	001
835*	1.04 ± 0.03	22.3	0.16	1.0 ± 0.1	000	1.95	16.8	23.6 | 2.2	00000	000
837*	1.15 ± 0.04	22.2	0.14	0.8 ± 0.1	000	1.98	22.1	23.6 | 2.3	00100	001
838	1.32 ± 0.12	21.9	...	...	00–	2.03	14.6	23.4 | 2.7	01010	001
840*	1.24 ± 0.09	22.1	0.10	...	000	1.95	1.8	23.2 | 3.2	00000	000
841	1.40 ± 0.09	21.8	0.15	...	000	1.94	9.5	23.1 | 3.6	–00–0	000
843*	1.11 ± 0.05	22.4	0.26	...	000	1.92	5.6	23.5 | 2.6	00000	001
845*	1.19 ± 0.15	21.7	0.28	0.8 ± 0.1	100	1.93	4.5	23.2 | 3.3	–00–0	000
846*	1.17 ± 0.07	22.0	0.25	...	000	1.95	3.3	23.3 | 2.9	00000	000
847*	1.03 ± 0.03	21.9	0.32	0.8 ± 0.1	001	1.93	7.9	23.1 | 3.5	00010	001
848*	1.24 ± 0.12	...	0.28	1.0 ± 0.1	0–1	1.88	13.9	23.2 | 3.3	–00–0	001
850*	1.05 ± 0.02	22.0	0.19	0.8 ± 0.1	000	1.93	12.3	23.3 | 3.0	00000	000
851*	1.12 ± 0.04	22.1	0.28	0.9 ± 0.1	000	1.89	5.0	23.2 | 3.4	00000	000
852*	1.38 ± 0.09	21.6	0.19	1.4 ± 0.2	000	1.99	3.6	23.4 | 2.7	01100	001
854*	1.20 ± 0.06	22.0	0.37	0.9 ± 0.1	001	1.88	9.0	23.2 | 3.3	20000	001
856*	1.05 ± 0.03	22.7	0.24	0.9 ± 0.1	001	1.91	7.0	22.8 | 4.7	–00–0	001
857*	1.10 ± 0.02	22.4	0.21	0.9 ± 0.1	000	1.95	14.8	23.5 | 2.6	00000	000
858*	1.25 ± 0.14	22.1	0.23	0.9 ± 0.1	000	1.98	5.5	23.1 | 3.7	–00–0	001
859*	1.18 ± 0.05	22.2	0.32	0.7 ± 0.1	001	1.93	3.7	23.0 | 3.9	00010	000
860*	1.04 ± 0.02	22.3	0.27	0.9 ± 0.3	001	1.91	20.4	23.1 | 3.4	00010	001
861	1.32 ± 0.13	22.2	...	...	00–	1.96	8.7	23.0 | 3.8	10010	001
862	1.09 ± 0.04	22.2	...	1.1 ± 0.1	00–	1.95	14.3	23.4 | 2.6	00000	001
863*	1.20 ± 0.06	22.3	0.19	0.9 ± 0.1	000	1.95	10.7	23.3 | 3.0	00010	001
864*	1.05 ± 0.02	22.4	0.20	...	000	1.96	6.7	23.5 | 2.6	00010	000
865*	1.02 ± 0.02	22.3	0.27	0.9 ± 0.1	000	1.93	13.0	23.4 | 2.8	00010	001
866*	1.08 ± 0.05	22.1	0.34	...	001	1.96	4.7	23.5 | 2.5	00000	101
867*	1.13 ± 0.01	22.1	0.39	...	001	1.96	16.4	23.2 | 3.3	00000	001
868	1.74 ± 0.13	21.5	0.15	...	110	2.01	12.2	23.0 | 4.1	01100	001
869	1.35 ± 0.01	22.0	0.22	...	000	1.92	5.8	22.9 | 4.4	00000	001
871	1.40 ± 0.04	21.7	...	...	00–	1.95	11.0	23.0 | 3.8	00110	000
872*	1.37 ± 0.05	21.7	0.22	1.0 ± 0.1	000	1.94	6.5	23.0 | 4.1	–00–0	001
874*	1.14 ± 0.05	21.8	0.31	0.8 ± 0.1	001	1.95	9.7	23.1 | 3.6	00010	001
877*†	1.10 ± 0.05	...	0.22	1.0 ± 0.1	0–0	1.94	5.1	22.9 | 4.3	10010	001
878*	1.37 ± 0.07	22.1	0.18	1.1 ± 0.1	000	1.91	4.1	23.5 | 2.5	00000	001
880	1.25 ± 0.07	22.0	...	0.9 ± 0.1	00–	1.91	8.7	22.8 | 4.9	00000	001
881*	1.17 ± 0.11	22.0	0.30	0.9 ± 0.2	000	1.96	5.3	23.2 | 3.4	–00–0	000
883*	1.13 ± 0.04	22.1	0.31	0.9 ± 0.1	001	1.90	2.6	22.7 | 5.1	00000	001
884	1.49 ± 0.13	21.8	...	...	00–	2.01	5.8	23.0 | 3.9	01000	101
885	1.15 ± 0.00	22.1	...	...	00–	1.93	12.4	23.3 | 3.1	–00–0	000
886	1.32 ± 0.09	22.0	0.19	0.9 ± 0.1	000	1.99	13.8	22.3 | 7.3	00011	001
887*	1.05 ± 0.01	22.2	0.29	0.8 ± 0.1	000	1.89	10.4	23.1 | 3.8	–00–0	001
888*	1.08 ± 0.05	21.9	0.41	...	001	2.01	1.3	23.1 | 3.8	01000	000
890*	1.02 ± 0.01	21.8	0.23	0.9 ± 0.1	000	1.94	10.8	23.4 | 2.9	–00–0	000
891	1.20 ± 0.03	22.1	...	...	00–	1.94	4.1	23.0 | 4.1	10110	000
893*	1.40 ± 0.21	21.8	0.15	1.0 ± 0.1	100	1.95	3.2	22.8 | 4.6	–00–0	001
894	1.03 ± 0.01	22.5	...	...	00–	1.98	8.0	23.1 | 3.7	10100	101
895	1.12 ± 0.03	21.9	...	...	00–	1.99	5.2	23.2 | 3.4	–00–0	001
896*	1.03 ± 0.02	22.3	0.14	1.4 ± 0.3	000	2.13	8.3	23.2 | 3.3	01100	000
898	1.20 ± 0.09	22.2	0.24	...	000	1.97	6.1	22.6 | 5.9	00100	000
901*	1.20 ± 0.10	22.1	0.25	1.0 ± 0.2	000	2.02	10.7	22.9 | 4.5	01010	000
902*	1.38 ± 0.14	21.7	0.21	1.1 ± 0.1	000	1.97	17.0	23.2 | 3.3	00010	001
903	1.26 ± 0.07	21.9	0.12	...	000	1.95	12.6	22.8 | 4.6	00010	000

Table 7. continued.

ID	airmass[a]	$\mu_{V,\mathrm{sky}}$[b]	A_V[c]	seeing[d]	flags(O)[e]	δ_λ[f]	S/N(R_{50})[g]	$I_{3\sigma}$[h]	flags(R)[i]	flags(C)[j]
904*	1.27 ± 0.08	21.7	0.22	1.3 ± 0.3	000	1.99	9.2	23.0 | 3.9	00000	101
909	1.29 ± 0.11	21.9	0.12	...	000	1.95	7.6	22.5 | 6.1	00000	001
910	1.28 ± 0.06	21.8	...	...	00–	2.05	6.8	23.0 | 4.0	–10–0	000
913	1.24 ± 0.10	22.1	...	...	01–	2.24	13.4	22.9 | 4.3	01100	001
914	1.16 ± 0.02	22.0	...	...	00–	1.92	12.4	23.2 | 3.4	00010	101
915	1.30 ± 0.11	22.0	...	...	00–	1.90	12.2	23.3 | 3.1	00010	001
916	1.21 ± 0.07	22.2	0.13	...	000	2.00	12.0	22.9 | 4.4	01010	000
917	1.12 ± 0.01	22.4	0.20	...	000	1.93	11.6	23.0 | 3.9	00010	001
922	1.23 ± 0.06	22.0	0.14	...	000	1.94	11.0	23.4 | 2.7	00000	100
924	1.32 ± 0.06	21.9	...	...	00–	1.94	10.4	23.3 | 3.1	00000	101
927	1.29 ± 0.05	22.0	0.11	...	000	1.98	3.9	22.7 | 5.1	00000	001
930	1.27 ± 0.05	21.9	...	...	00–	1.90	7.8	23.5 | 2.4	00000	000
932	1.29 ± 0.05	21.8	0.12	...	000	1.95	10.6	23.3 | 3.0	00000	001
935*	1.09 ± 0.06	22.3	0.18	...	000	2.13	4.5	23.4 | 2.8	01100	000
936	1.45 ± 0.13	21.6	...	...	00–	1.94	7.0	23.0 | 3.9	–00–0	001
937	1.16 ± 0.04	22.1	0.19	...	000	1.98	7.1	23.2 | 3.2	–01–0	101
938	1.13 ± 0.07	...	0.23	1.0 ± 0.1	0–0	1.94	12.6	23.4 | 2.8	00000	000
939*	1.32 ± 0.08	21.9	0.28	0.9 ± 0.1	001	1.89	5.2	23.3 | 3.0	–00–0	000

Notes. We describe the meaning of each column including the identifier of each column in the electronic table available on the DR2 web page. [a] Mean airmass (OBS_AIR_MEAN) and rms (OBS_AIR_RMS) of the observations for the frames used to create the considered datacube. [b] Average night-sky surface brightness (OBS_SKY_MAG) in the *V* band during the observations in units of mag arcsec^{-2}. [c] Average night-sky attenuation (OBS_EXT_MEAN) in the V band during the observations in magnitudes. [d] Average natural seeing (OBS_SEEING_MEAN) in the V-band during the observations in arcsec (FWHM). [e] Observation quality flags, combining the three individual column flags (FLAG_OBS_AM, FLAG_OBS_SKYMAG, FLAG_OBS_EXT) as described in Sect. 5. [f] Average spectral resolution (RED_DISP_MEAN) in Å (FWHM), measured by fitting the night-sky emission lines with single Gaussian functions. [g] Average signal-to-noise ratio (CAL_SNR1HLR) estimated for the full wavelength range at one half light radius from the center. [h] Average flux at the 3σ continuum detection limit in units of B-band mag arcsec^{-2} and in units of 10^{-18} erg s^{-1} cm^{-2}Å^{-1} arcsec^{-2}. [i] Reduction/instrumental performance quality flags, combining the five individual column flags (FLAG_RED_STRAYLIGHT, FLAG_RED_DISP, FLAG_RED_CDISP, FLAG_RED_SKYLINES, FLAG_RED_LIMSB) as described in Sect. 5. [j] Quality control CAL flags, combining the three individual column flags (FLAG_CAL_SPECPHOTO, FLAG_CAL_WL, FLAG_CAL_IMA) as described in Sect. 5.

Appendix A: Computing the error spectrum for co-added spectra

Some science cases require a minimum S/N in the spectra, specially in the outer parts of the galaxies. This is achived by spatially co-adding spaxels in the datacubes, often by means for an adaptive binning method like the Voronoi-binning scheme, implemented for optical IFS data by Cappellari & Copin (2003). However, the final error spectrum of the co-added spectra cannot be simply quadratically summed since the spectra are not independent of each other. As described in Sect. 3.1, we adopt an inverse-distance weighted image reconstruction and, like many other image resampling schemes it introduces correlation between the spaxels in the final datacube. In Sect. 3.2 we provide a equation that relates the analytically propagated error store in the datacubes with the final "real" error of the co-added spectra[10].

Let B be a bin of size N spectra, i.e. we want to co-add N spectra and compute the corresponding error spectrum for that bin. Since we are adding the flux to obtain an integrated spectra, first we need to add quadratically the errors of each individual spectra:

$$\epsilon_B^2 = \sum_{k=1}^{N} \epsilon_k^2$$

This would be the error spectrum of the bin B if the spaxels where completely independent. To account for the correlated noise, we just need to multiply by the corresponding "correlation factor" (Eq. 1) for a given number of spectra in a particular bin:

$$\epsilon_{\mathrm{real,B}}^2 = \beta(N)^2 \times \epsilon_B^2$$

When the bin B contains a large number of pixel ($N \gtrapprox 80$), the use of Eq. 1 is not recommended. In this case, the ERRWEIGHT HDU extension of the CALIFA FITS file datacube should be used (see Table 2) as a correction factor for each spaxel.

[10] See also Sect. 3.2 and 3.3 of Cid Fernandes et al. (2013) for a detailed disquisition on error propagation and correlated noise for IFS.